



**HAL**  
open science

# Effect of cross-section on flow three-dimensionality for prismatic bodies and the associated noise emission

Wagner Pinto, Florent Margnat, Yves Gervais

► **To cite this version:**

Wagner Pinto, Florent Margnat, Yves Gervais. Effect of cross-section on flow three-dimensionality for prismatic bodies and the associated noise emission. 25th AIAA/CEAS Aeroacoustics Conference, May 2019, Delft, Netherlands. pp.2019-2531, 10.2514/6.2019-2531 . hal-04443850

**HAL Id: hal-04443850**

**<https://univ-poitiers.hal.science/hal-04443850v1>**

Submitted on 7 Feb 2024

**HAL** is a multi-disciplinary open access archive for the deposit and dissemination of scientific research documents, whether they are published or not. The documents may come from teaching and research institutions in France or abroad, or from public or private research centers.

L'archive ouverte pluridisciplinaire **HAL**, est destinée au dépôt et à la diffusion de documents scientifiques de niveau recherche, publiés ou non, émanant des établissements d'enseignement et de recherche français ou étrangers, des laboratoires publics ou privés.

Copyright



# Effect of cross-section on flow three-dimensionality for prismatic bodies and the associated noise emission

Wagner J. G. S. Pinto\*, Florent Margnat† and Yves Gervais‡

*Institut Pprime, Département Fluides, Thermique, Combustion - Université de Poitiers, ISAE-ENSMA, CNRS - Bât. B17  
6 rue Marcel Doré TSA 41105, 86073, Poitiers Cedex 9, France*

**The influence of the geometry of prismatic bodies on their aerodynamic sound emission is studied. Curle's formalism links the noise level to lift fluctuation and the spanwise organization of the flow coherent structures. Here, the acoustic field is measured using a set of microphones, and the flow spanwise coherence length is estimated from hot-wire velocity signals. An equivalent lift fluctuation is educed from the usual procedure of extrapolation of the sound level from 2D simulations to 3D long-span bodies. Circular and rectangular - of sectional aspect ratios (breadth-to-height ratio  $AR = b/d$ ) of 1, 2 and 3 - cross sections are tested for a Reynolds number range from 6,000 to 27,000. The closure of the problem and the influence of the geometry are addressed by confronting the educed lift coefficients to literature values at Reynolds numbers in the same range, and in the 2D laminar regime. Microphone measurements show that all over the tested flow velocities, the acoustic efficiency of the cross sections respects the following hierarchy: circular <  $AR = 2$  < square <  $AR = 3$ . The coherence length at the vortex shedding frequency is around  $5d$  for the circular and square sections, while it is around  $20d$  for the two rectangular sections. Educed lift fluctuation values are found to be lower than those previously reported, and of the same order than those obtained in the 2D laminar regime. The flow spanwise coherence length at the vortex shedding frequency is found to be inversely proportional to the breadth based, RMS, educed lift coefficient.**

## I. Introduction

### A. Noise generation by flow over prismatic bodies

**T**HE aerodynamic noise production of prismatic bluff bodies is described to be originated from the axially distributed, periodic surface pressure fluctuations [1–3] due to the Von-Karman vortex shedding. Once the flow is not completely phased in the spanwise direction, the three dimensional flow organization and its associated coherence is an important element in the construction of the sound emission. This spatial parameter is intrinsically associated with the flow conditions and the shape of the geometry, thus setting the context where this work is placed.

While many studies are exclusively focused on the circular cylinder, some works that evaluated the noise emission of different prismatic bodies can be found: the study of wall-mounted geometries performed by Becker et al. [4], who used a square cylinder combined with elliptical and triangular wedges and afterbodies; King & Pfizenmaier [5], who studied a set of different cross-sections (circular, elliptical, rectangular) and cylinder lengths; Moreau & Doolan [6], who evaluated the flow and noise emission of wall-mounted circular and square cylinders of multiple lengths; Iglesias et al. [7], also for elliptical and rectangular prisms, and mostly focused on the influence of the yaw angles aiming at the application to pantographs noise prediction [8]; and more recently, Octavianty et al. [9], who studied different rectangular sections and also performed the measurements of the spanwise flow distribution.

For studies of long cylinders (length/diameter > 10, considering the results in [5]), not much is measured in terms of aerodynamics. In the other way, for small wall-mounted geometries, a fine description of the flow field is performed, sometimes using optical measurements techniques such as PIV. However the results obtained in the later are mostly defined by the end-conditions, rather limiting its conclusions to that given geometrical category.

Considering the deduction by Fujita [10], derived from the developments of Curle [1] and Philips [2], the RMS value of the acoustic pressure fluctuation may be estimated as:

\*PhD student, Fluids, Thermal and Combustion Sciences Department, wagner.goncalves@univ-poitiers.fr.

†Assistant Professor, florent.margnat@univ-poitiers.fr

‡Professor, yves.gervais@univ-poitiers.fr

$$\overline{P}^2(r) = \frac{\rho^2 U_\infty^6 \text{St}^2 \ell L_c C_L'^2}{16c^2 r^2} \left[ 1 + \left( \frac{\lambda}{2\pi r} \right)^2 \right] \quad (1)$$

where  $P$  is the acoustic pressure,  $\rho$  is the air density,  $U_\infty$  is the flow inlet velocity,  $\text{St}$  is the Strouhal number,  $\ell$  is the cylinder's length,  $L_c$  is a coherence length,  $C_L'$  is the RMS lift coefficient,  $c$  is the sound velocity and  $\lambda = c/f_{\text{peak}}$  is the acoustic wave length. The second fraction on the right side is defined as the near-field contribution. This equation shows that, for a fixed flow condition, the acoustic pressure ( $\overline{P}^2$ ) is derived from a combination of the Strouhal number ( $\text{St}$ ) and lift fluctuation ( $C_L'$ ), distributed axially by a spanwise coherence ( $L_c$ ).

## B. Acoustic and coherence measurements

This work presents experimental results for both sound and coherence. A similar approach is present in [9] with the calculation of the spanwise correlation, but the conclusions are limited to the association of the correlation length to the broadness of peaks in the sound spectra. For the complete closure of the problem, it would be necessary to also perform the measurements of the aerodynamic efforts fluctuations [11].

The main objective of this work is the analysis of the cross-shape influence in the aeolian tone production. For that, circular cylinder and prisms of rectangular sections of different aspect ratios (breadth/height) are tested. Such set of geometries has gotten attention for both its noise emission (at high Reynolds on previously cited references [5, 7, 9] and at low Reynolds in [12, 13]) and aerodynamic behavior (for instance, [14–17]). Although the increase of the breadth causes a reduction of the strength of the vortex [16] and a discontinuity in the vortex shedding frequency [15], the noise emission presents an increase. The origins of that difference remain unclear and are investigated in this paper.

The acoustic pressure is measured with an array of microphones placed above the cylinder, while the coherence is measured using two hot-wire probes. As discussed in [18, 19], velocity based coherence values are a representative estimator of the pressure and lift coefficient coherence. Present measurements are described in details in a previous document [20]. One of the advantages of the results in this work is to remain at fixed geometrical conditions for all the tested shapes, that is, the geometry height and spanwise extent are fixed. That means that empirical or simplified correction formulations are nonexistent.

## C. From lift coefficient estimation to noise generation mechanisms

Accessing the unsteady wall pressure values is a complex task and involves either the use of surface pressure taps that limit the size of the cylinder bodies (bigger sections, resulting in larger Reynolds numbers and lower vortex shedding frequencies), thus provoking issues associated with Reynolds number and sound frequency ranges, or by using aerodynamic balances, problematic when different geometries are to be used once it would demand a series of calibrations and sensibility studies. In order to get the corresponding aerodynamic efforts, a statistical correction procedure based on the Curle's analogy is considered, for a compact source and an observer located in the far-field. From the principle of a normally distributed spanwise flow, and accounting for an equal magnitude and only de-phased contribution of small segments, Seo & Moon [21] proposed a procedure for the correction of sound emission for a long cylinder based on the reasoning found in the previous works of Kato et al. [22] and Pérot et al. [23]. Current application is based on the procedure of Doolan [24], that reconstructed the sound spectra generated by a circular cylinder from data of a 2D URANS simulation. Thus, the procedure here is applied backwards, that is, from the final sound emission and the measured coherence length, a sectional behavior is estimated.

The document is presented as follows. Section II is dedicated to the acoustical part of the study, with the description of the experimental setup and the data processing techniques that are used (II.A), the obtained results in terms of sound spectra, sound directivity, and velocity exponent (II.B) and a conclusion around the influence of the cross-section on the sound signature of bluff bodies (II.C). Influence of shape on flow is presented on Section III, with the analysis of measured velocity signals (III.A) and of the spanwise flow axial coherence (III.B). Section IV contains the presentation of the statistical correction method (IV.A), a sensitivity study (IV.B) and the procedure for the deduction of RMS lift coefficients (IV.C). Analysis of how the Reynolds number, shape, lift fluctuation and spanwise topology relate and the results of that mechanics in sound emission are present on Section V, with the dissection of the measured noise regarding each parameter contribution (V.A) and a comparison with the literature and discussions over the deduced lift RMS coefficients for the circular (V.C.1) and rectangular (V.C.2) sections. Section VI closes the document with an extended discussion and the conclusions. All the integral acoustical results, including peak, band and overall sound pressure levels for all tested velocities and shapes are listed on the appendix.

## II. Influence of shape on the acoustic field

### A. Setup and data processing

#### 1. Wind tunnel and studied shapes

An experimental analysis is performed in the anechoic wind-tunnel BETI of Institut Pprime at Poitiers, France, represented in Fig. 1. It is a closed circuit, with an exit nozzle of section  $70 \text{ cm} \times 70 \text{ cm}$ , contraction factor of 10:1, maximum velocity of 50 m/s. The anechoic chamber cutoff frequency is of 200 Hz.



**Fig. 1** Photography of the anechoic chamber of the wind-tunnel BETI - Institut Pprime, France.

The test cases are elongated bluff bodies of different cross sections of fixed height  $d$  that equals 10 mm. It is the reference length for the calculation of the Reynolds ( $Re = U_\infty d / \nu$ ) and Strouhal ( $St = f d / U_\infty$ ) numbers; sectional breadth  $b$  is not maintained. The shape of the sections are the following (illustrated in Fig. 2): a circular cylinder of diameter 10 mm; a square section of side 10 mm; a rectangular sections of dimensions 10 mm  $\times$  20 mm; and a rectangular section of dimensions 10 mm  $\times$  30 mm. The sectional aspect ratio ( $AR = b/d$ ) is of 1, 1, 2 and 3, respectively. The center of the cylinder is placed 30 cm downstream of the nozzle outlet, connected at the extremities to beams under the wind-tunnel convergent. Geometrically, the cylinders are 86 cm long (available length between the supports). Considering only the part immersed in the flow, the effective length is of  $\ell = 70 \text{ cm}$  ( $\ell/d = 70$ ). To the best of the authors' knowledge, such spanwise extent has not been considered before, and allows an unbiased estimation of the spanwise intrinsic flow organization with negligible end effects.

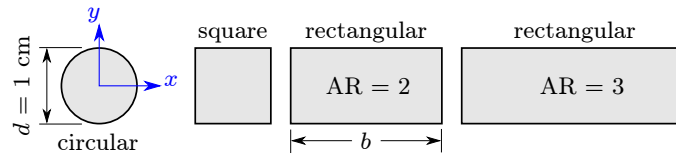


**Fig. 2** Tested cross sections (in scale), aspect ratio defined as  $AR = b/d$ . Flow from left to right.

The cylinders of circular and rectangular section of  $AR = 3$  are solid while the others are hollow. All bodies are made of aluminum with the exception of the widest rectangle that is made of steel. Prismatic body surfaces are smooth and corners are sharp; although small damages can be noted, no treatment was performed concerning the later two aspects and the present defects are considered negligible. Preliminary tests were performed with carbon fiber bars, but the obtained noise values were overestimated due to the resonance frequency lying at the range of the obtained vortex shedding.

Flow velocities in the range of 10 m/s to 40 m/s are used. The turbulence intensity measured at the location of the center of the cylinder with empty test section is of 0.5%. The room temperature is also measured at each measuring session, with an average temperature oscillating from 17.4 to 22.8 degrees Celsius. For simplicity, air properties are

fixed and taken as follows: air density of  $\rho = 1.225 \text{ kg/m}^3$ ; sound speed of  $c = 340 \text{ m/s}$ , so the Mach number  $M = U_\infty/c$  ranges from 0.03 to 0.12; and air kinematic viscosity of  $\nu = 1.5 \times 10^{-5} \text{ m}^2/\text{s}$ , leading to a range of Reynolds numbers from 6,667 to 26,667.

The flow and noise are measured by the use of hot-wire anemometry and microphone measurements. Once the presence of the hot-wire probes are disturbing to the acoustic field, the procedures are performed separately. Detailed descriptions of each experimental setup and the associated post-processing techniques are presented next, in the same section as their respective results.

## 2. Acoustical measurements

A 7-microphone array is placed above the cylinder (see illustration on Fig. 3). The microphones are spaced by 15 degrees, placed at the spanwise center of the cylinder at a distance of  $r = 1 \text{ m}$  (that is 1.42 times the cylinder's length), allowing directivity measurements. The first microphone forms an angle of 45 degrees with the incoming flow and microphone number 4 is at  $90^\circ$ . The sampling frequency is of 12.8 kHz for a recording time of 60 seconds. Sound spectra are calculated using the Welch's method, with 8192 points and 90% overlap, leading to a spectral precision of  $\Delta f = 1.56 \text{ Hz}$ . No weighting is applied in the calculation of the sound pressure levels indicated in this work. Decibel levels are calculated as  $10 \log_{10}(\bar{P}^2/P_{\text{ref}}^2)$ , being  $\bar{P}$  the averaged Fourier transform of the acoustic pressure and  $P_{\text{ref}} = 20 \mu\text{Pa}$  the reference pressure.

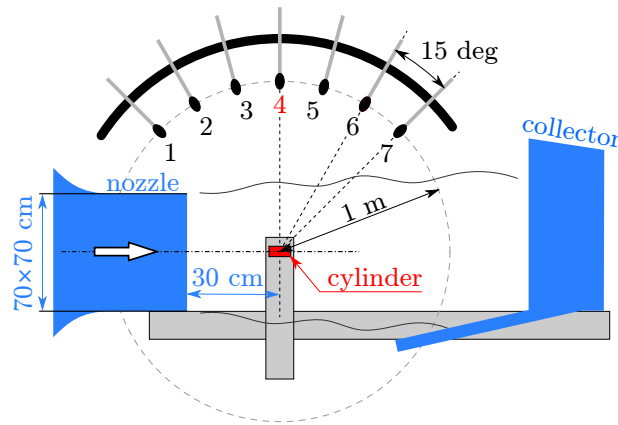


**Fig. 3** Diagram of the experimental setup with the microphone array. The lower wall of the collector is extended in order to adapt the setup for a fully open jet configuration.

Unless otherwise stated, presented sound spectra were corrected for background noise, based on recordings performed without the cylinders. Performed correction accounts only for wind-tunnel noise and do not deal with undesirable aerodynamic effects related to the existing mixing layers, that are considered negligible. Examples of the magnitude of such corrections can be found in [7].

Considering an observer at a distance  $r$  from the source, Eq. (1) applies to geometrically ( $\ell \ll r$ ) and acoustically ( $\ell \ll \lambda$ ) compact bodies, for an observer located in the far field ( $r \gg \lambda$ ). For the vortex shedding frequency, considering a ratio of one, respect of the latter 2 conditions for the current measurements are listed on Table 3. The acoustic compactness criterion is respected for 83% of the measurements, while the far-field condition only for 38%. Albeit the fact that the microphones may not be placed in the far-field, the near-field component at the peak, evaluated as presented in Eq. -(1), remains lower than 2 dB and is considered negligible (values also listed on Table 3).

In order to calculate the overall sound pressure level, three procedures were tested: integral for  $f > 80 \text{ Hz}$ ;  $f \in [100, 1000] \text{ Hz}$ , same procedure used by King and Pfizenmaier [5]; and integral for the complete spectra (from 0 to 6400 Hz). As the results from the first two procedures are barely modified, notably no remarkable effect on the velocity exponents was obtained, the components at low frequency and high frequencies are, as expected, negligible. Thus, to avoid setting arbitrary thresholds, the levels obtained from the complete spectra ( $f \in [0, 6400] \text{ Hz}$ ) are used on the study. Obtained values are listed on appendix, Table 3, for the central microphone, for all sections and flow velocities. The fundamental peak level and the level considering a band around the peak are also presented.

## B. Acoustic results

A description of the obtained acoustical results is presented on this section. First, a comparison of current values for the circular cylinder to previous works is performed in order to qualify the obtained results. Second, the analysis of the acoustical response of the studied geometries is expanded in terms of sound spectra, velocity exponent and directivity, with a systematic discussion around the influence of the cross-section.

### 1. Validation - Circular cylinder

A comparison of the obtained noise spectra with literature data is performed for the circular cylinder and presented in Fig. 4. There is a constant offset between the experiments for the sound pressure levels (Fig. 4a). The observed behavior is a consequence of different experimental conditions (cylinder's length and diameter and flow velocity and Mach number), and experimental setup, notably the presence of end-plates at the nozzle extremities in the works used as reference [25, 26]), and observed similitude in the levels are just coincidence. In terms of frequency content, considering the difference of the spectral distribution to the peak level (Fig. 4b), the similarity of the curves is shown. The values around the first peak are slightly lower than those observed in previous works, what may be associated to the slightly smaller Reynolds number. The prominence of 30 dB of the fundamental mode, as well as the shape of the curve at the first 2 harmonics are comparable in all studies.

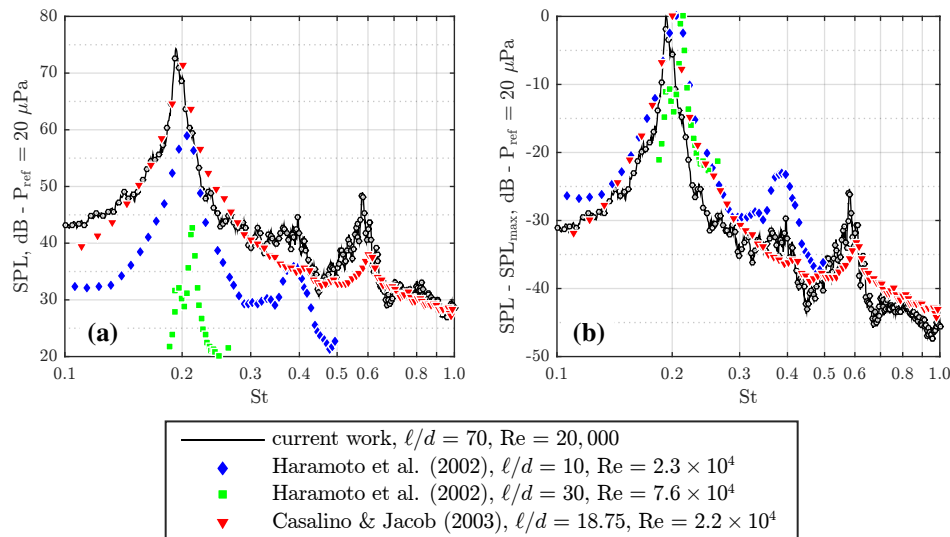


**Fig. 4** Spectral distribution of the sound pressure level (a) and relative sound pressure level (b) of the emission of the circular cylinder. Current work data are not corrected for background noise and circle markers are added every 12.5 Hz for visual aid. Comparison with data from the literature [25, 26].

One-third octave scaled levels are presented on appendix, Fig. 21.a for the circular cylinder. Once again, the difference of cylinders' length ( $l/d$ ) and flow velocities provokes the offsets for both the level and the frequency. However, the shape of the curves is quite similar to previously reported results [7, 27], especially in what concerns the prominence of the sound contribution at the peak frequency compared to the other frequency bands.

A sample of the obtained 1/3 octave SPL distributions for all the geometries tested in this work is presented in Fig. 21.b. The curves follow a similar trend for all sections, being the level of the band of the peak frequency around 20 dB higher than the rest of the spectrum. Like in the literature, the square section is louder than the circular one [5, 7].

The acoustic signatures of the different cross-sections are compared next by analyzing the sound pressure spectra, the width of the spectral band around the peak, the sound directivity and the exponent of the sound pressure dependency to the inlet velocity. A table containing the peak frequencies and sound levels (peak, overall and band) is present in the appendix.

## 2. Sound spectra

**Peak frequencies and peak levels** First, sound spectra are presented in Fig. 5 for the multiple flow velocities that are tested, for the central microphone ( $\theta = 90^\circ$ ). As noted in previous works, the square is louder than the circular section [5–7]. At the peak frequency, the current hierarchy is observed: circular cylinder < rectangular cylinder of aspect ratio 2 < square cylinder < rectangular cylinder of aspect ratio 3. The prominence of the first and second harmonics follow the same hierarchy, that is less noticeable for the circular cylinder and easily remarked for the widest rectangular section. For all the geometries, the peak Strouhal number (listed on Table 3 in the appendix) is rather unmodified with the flow velocity.

For  $U_\infty = 10$  m/s, the tone associated with the vortex shedding is under the anechoic chamber cut-off frequency of 200 Hz for all geometries, thus this is not considered for most of the analysis performed in this work. Due to a reduced peak Strouhal number, this is also the case for most velocities for the rectangle of AR = 2.0, thus results for that section are not as reliable as what is obtained for the other geometries.

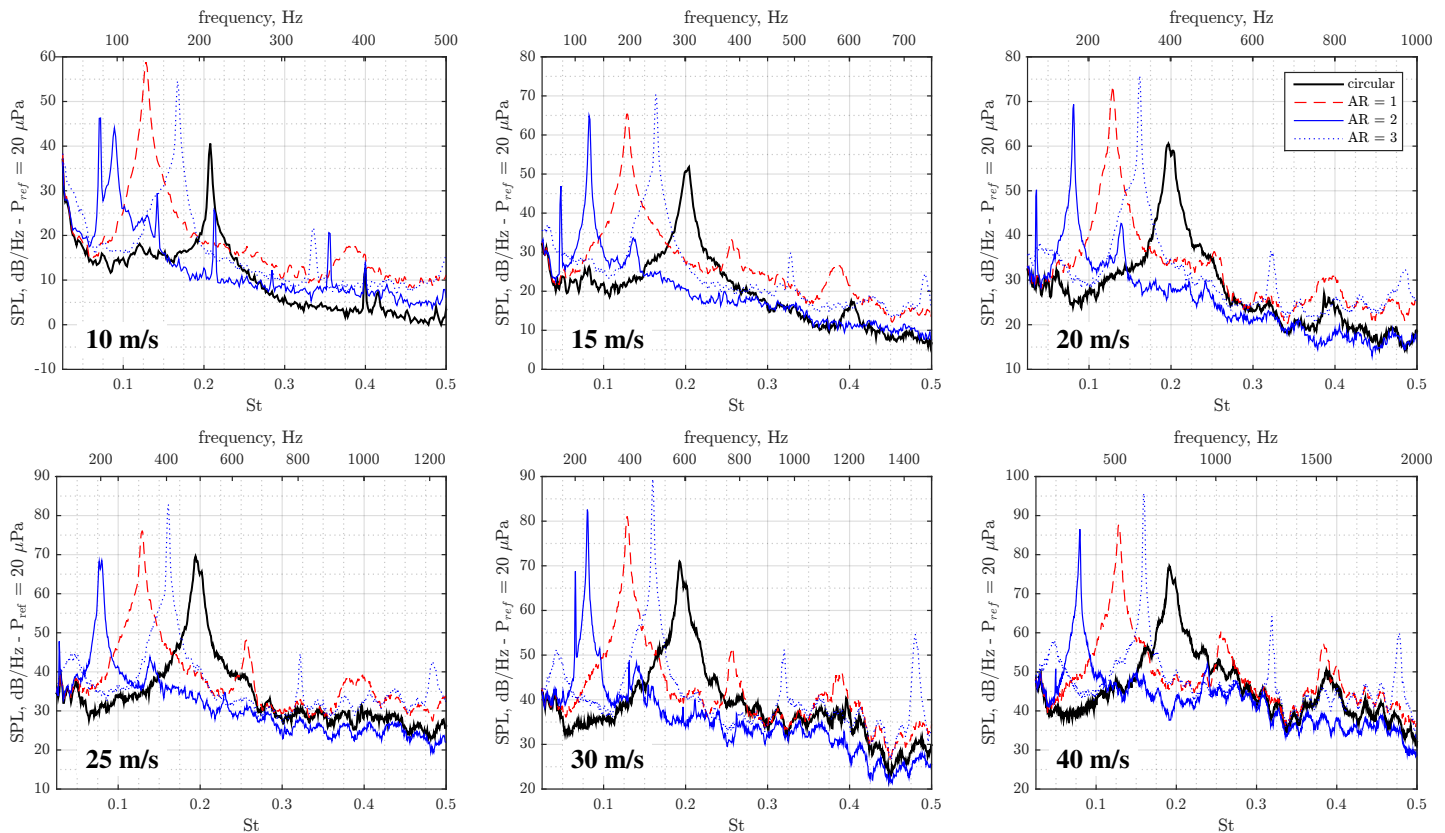


**Fig. 5** Sound spectra for all tested cylinders at different flow velocities, microphone at 90 deg of the flow.

Two peaks for AR = 2, at  $St \approx 0.08$  and  $St \approx 0.14$  are due to the existence of two vortex shedding modes for that given geometry. The first and most energetic one is associated with the flow separation at the upstream vertex, similarly to what happens for the square section, while the later corresponds to the vortex shedding happening at a downstream position due to the reattachment of the flow on the upper and lower faces of the prism, as observed for the rectangle of AR = 3. This transition creates a discontinuity on the  $St \times AR$  curve and is present in several works in the literature, such as [14, 16, 28]. From the analysis of the velocity field spectra performed in an earlier work [20], the two modes are believed to coexist. The origin of the narrow peak on the left of the vortex shedding one is unknown.

**Peak width** Differences regarding the width of the peaks can also be seen on Fig. 5. Considering the definition of the pressure level band (frequency range for which the level is greater than peak level - 10 dB), evolution of the obtained peak widths are illustrated on Fig. 6. Except for the lowest velocity, the peak is almost of constant size for the circular

cylinder, fluctuating around  $\Delta St = 0.017$ . For the rectangular sections, the band size decreases with the Reynolds. The high width for  $AR = 2.0$  at  $U_\infty = 25$  m/s is associated to the merge of two peaks.

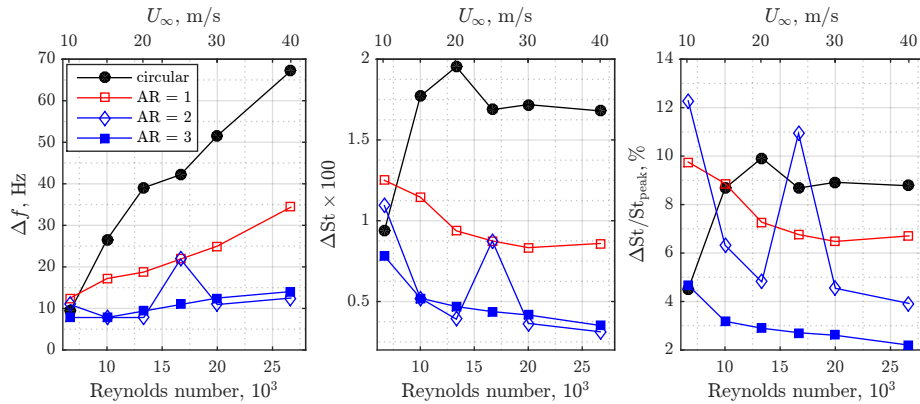


**Fig. 6 Evolution of peak width for multiple cross-sections considering the frequency range delimited under 10 dB of the peak frequency: in frequency (left), in St (center) and percentage of the  $St_{peak}$ .**

The noted trend is an indication that the evolution of the flow is different regarding the shape of the geometries and the presence of sharp edges. For the circular cylinder, there is no significant change in the shape of the spectrum, implying that the experimented flow regime is well established at the tested range. For the rectangular sections, a change in the velocity is more capable of modifying the sound spectrum, and peaks are narrower at larger Reynolds number. This results is the opposite of what could be deduced from classical turbulence development deduction, and shows that the difference of cross-section is an important factor in the behavior of the flow and the cylinder aeroacoustical response.

### 3. Directivity

The sound directivity is illustrated in Fig. 7 with the difference between the level for each microphone and the level of the central one ( $\theta = 90^\circ$ ), considering the peak sound pressure level. For the first microphones, the shape of the curve is relatively respected; for microphones after  $90^\circ$ , measured pressure levels are higher than expected. This result is believed to be due to the flow, that can freely expand, what may perturb the pressure fluctuations that are captured by the microphones downstream  $90^\circ$ , and to sound waves reflections, notably at the convergent.

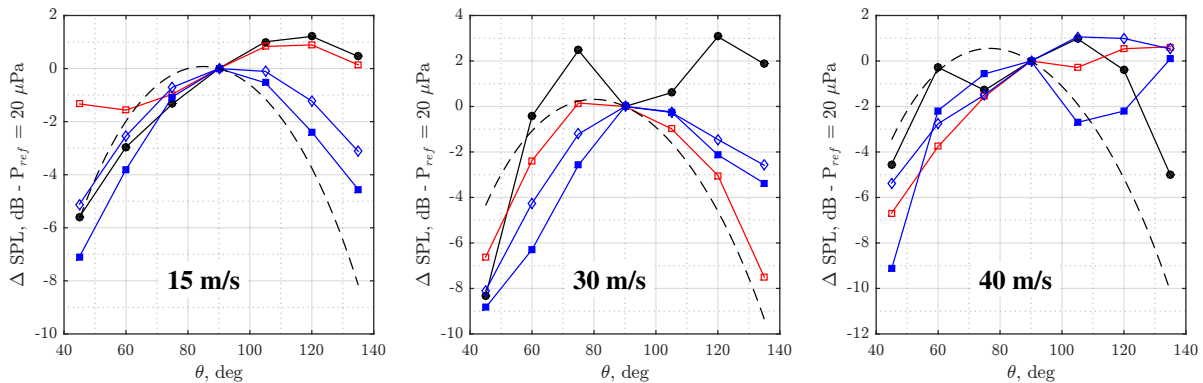


**Fig. 7 Sound directivity for all tested cross-sections at different flow velocities, peak sound pressure levels, same legend as in Fig. 6. Hatched line represents the analytical dipole corrected by the flow [29].**

### 4. Sound level velocity exponent

The sound pressure level evolution with the velocity is presented in Fig. 8, for the four cross-sections and the microphone at  $90^\circ$ . The peak value ( $SPL_{peak}$ ) and the full spectrum (OASPL, integral of the power spectral density

from 0 to 6400 Hz) are selected and the least-squares linear regression law is presented. For both quantities and all sections the levels evolve exponentially with an exponent close to 6, as deduced by Curle [1], evidencing the dipolar and compact nature of the emissions. Tests without the background correction returned the same exponents. Once more, values at  $U_\infty = 10$  m/s slightly deviate from the tendency, for example for  $AR = 2$ , and spoil the regression line when considered. Thus, the corresponding velocity exponents and curves presented in Fig. 8 do not consider the measures at that flow velocity.

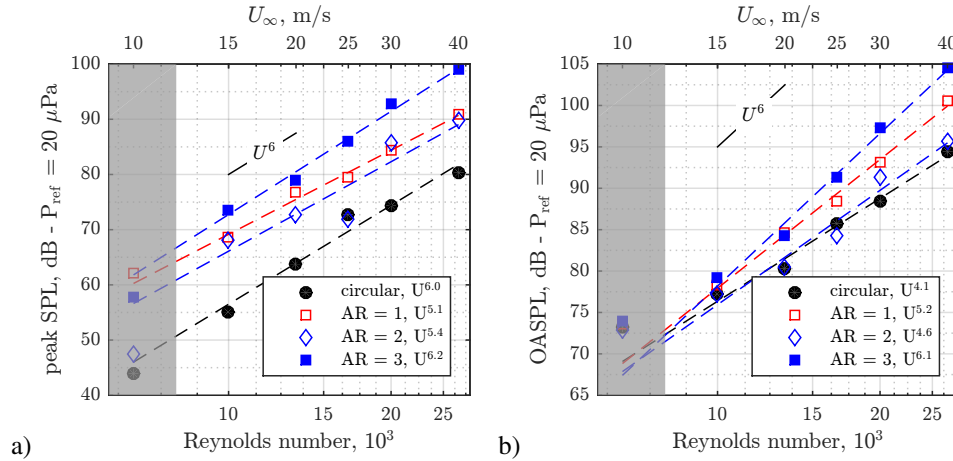


**Fig. 8** Evolution of the sound pressure level as a function of the Reynolds number for: (a) level at the peak frequency; and (b) the integral of power spectral density (0 - 6400 Hz, OASPL). The points corresponding to  $U_\infty = 10$  m/s are not considered when calculating the regression laws that are displayed.

### C. Conclusion about shape influence from acoustical measurements

It is concluded that the modification of the cross sections results in remarkable changes on the sound spectrum features and absolute sound pressure level. However, in terms of the tonal character and the evolution with the flow velocity, all tested sections have a dipolar trait and respect Curle's analogy despite the disturbances noted for the velocity exponent and directivity patterns, also noted in literature values [5, 7].

Considering the central microphone, the evolution of the overall sound pressure levels with the aspect ratio of the rectangular sections is presented on Fig. 9. Plotted values are centered at the average of the difference between the OASPL for the rectangle and the square section calculated for each flow velocities (see Table 3), error bars representing the limits.

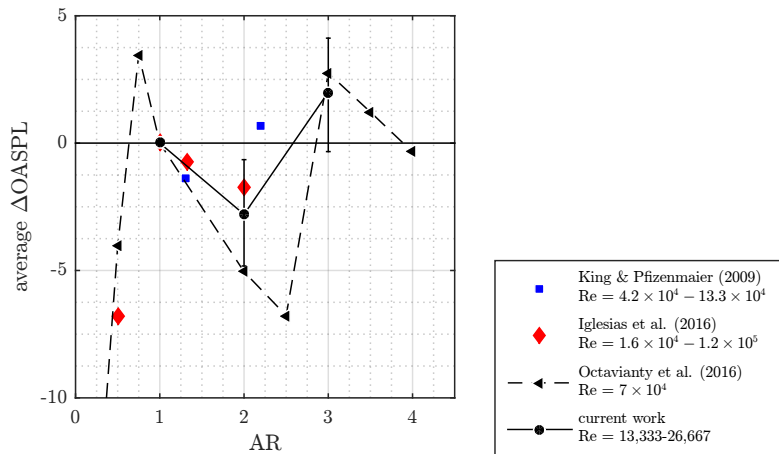


**Fig. 9** Evolution of overall SPL with aspect ratio, difference to the level obtained for the square section [5, 7, 9].

The behavior noted here is the same than presented in previous works: a decrease from the square to  $AR = 2$  and a increase from  $AR = 2$  to  $AR = 3$ ; the circular cylinder is, for all velocities, the quietest shape. Octavianty et al. [9] associated the shape of the curve OASPL versus  $AR$  to the modification of the peak Strouhal number, noting the similarity between the two curves. Same conclusion was not possible with current data. In order to understand such a behavior, further discussion on the origins of those disparities is made possible from coherence measurements and is presented next.

### III. Influence of the shape of the bodies on the velocity field and spanwise organization

The aerodynamic behavior of the flows are quantified using hot-wire measurements. Experiments are performed in the same installation used for the acoustic measurements II.A. The present application of the hot-wire technique is described in details in [20]. In particular, the probe position is set based on the mean flow, allowing fair comparisons between geometries. Analysis of velocity signals and flow spanwise coherence are presented next.

#### A. Velocity signals

The analysis of velocity signals provide a first hint on the influence of the cross section shape, and allows the setting of the turbulence time scale used in the correction method on Section IV.A.

##### 1. Normalized signals and PDF

Examination of the fluctuating velocity can highlight some aspects of the vortex shedding. A portion of the normalized velocity signals and the probability density functions (PDF) of the complete recordings are presented on Fig. 10 and 11. The amplitude of the velocity is normalized by its RMS value and the time by the period of the vortex shedding cycle  $T = 1/f_{\text{peak}}$ . For the rectangular section of  $AR = 2$ ,  $St_{\text{peak}} = 0.08$  is considered.

Same analysis is performed by Norberg [19], considering surface pressure measurements for a circular cylinder. Current velocity signals are similar in both form and distribution, including the negative skewness and the intermittent low amplitude excitation (the starting point is chosen arbitrarily such as to place the event at the center of the time scale in Fig. 10 and 11), that are associated by Norberg with near-wall vortex dislocations.

It is striking that these normalized velocity signals are strongly changed by the cross section shape. The flow around the square section hardly differs from the flow around the circular cylinder, visible in both the signal amplitudes and the probability distribution. For  $AR = 2$ , velocity values are more random, as it can be seen by the shape of the PDF, almost identical to a normal distribution, and the existence of two tones is visible in the time evolution with the presence of interchanged peaks of different magnitudes. The longest rectangular section ( $AR = 3$ ), presents, at both velocities, two clear peaks in its PDF (in a smaller scale, distorted peaks can also be seen for the square and circular sections). Norberg [19] associated that density shape to a sine wave with random noise.

We note that the obtained PDF are modified when different positions are taken in account. The represented results were chosen due to the consistency with the position used in the following sections of the article and also because they were the most repeated distribution.

##### 2. Turbulence time scale

The turbulence time scale defined by Doolan [24] is based on the duration of  $10 T$  of the low amplitude events signalized by Norberg [19]. The same behavior is noted in current results for the circular cylinder. Equal value is admitted to the other cross-sections that are studied, however it is clear that further analysis should be performed for the description and quantification of the phenomenon. Owing to the limitations of the available data, this first approximation is used for the rest of this document.

These observations lead to an initial discussion about the difference behavior due to the modification of the cross-section. The velocity signal footprint is quite similar for both short sections. The transition for  $AR = 2$  that creates the discontinuity of the peak Strouhal number is also associated with an increase in the randomness of the signal. In the other direction, the longest section has a rather clean velocity signal, indicating a flow less affected by turbulence. As a first conclusion, the influence of the shape can be associated with a different state in terms of flow development, working similarly to a modification of the Reynolds number, as discussed in [20].

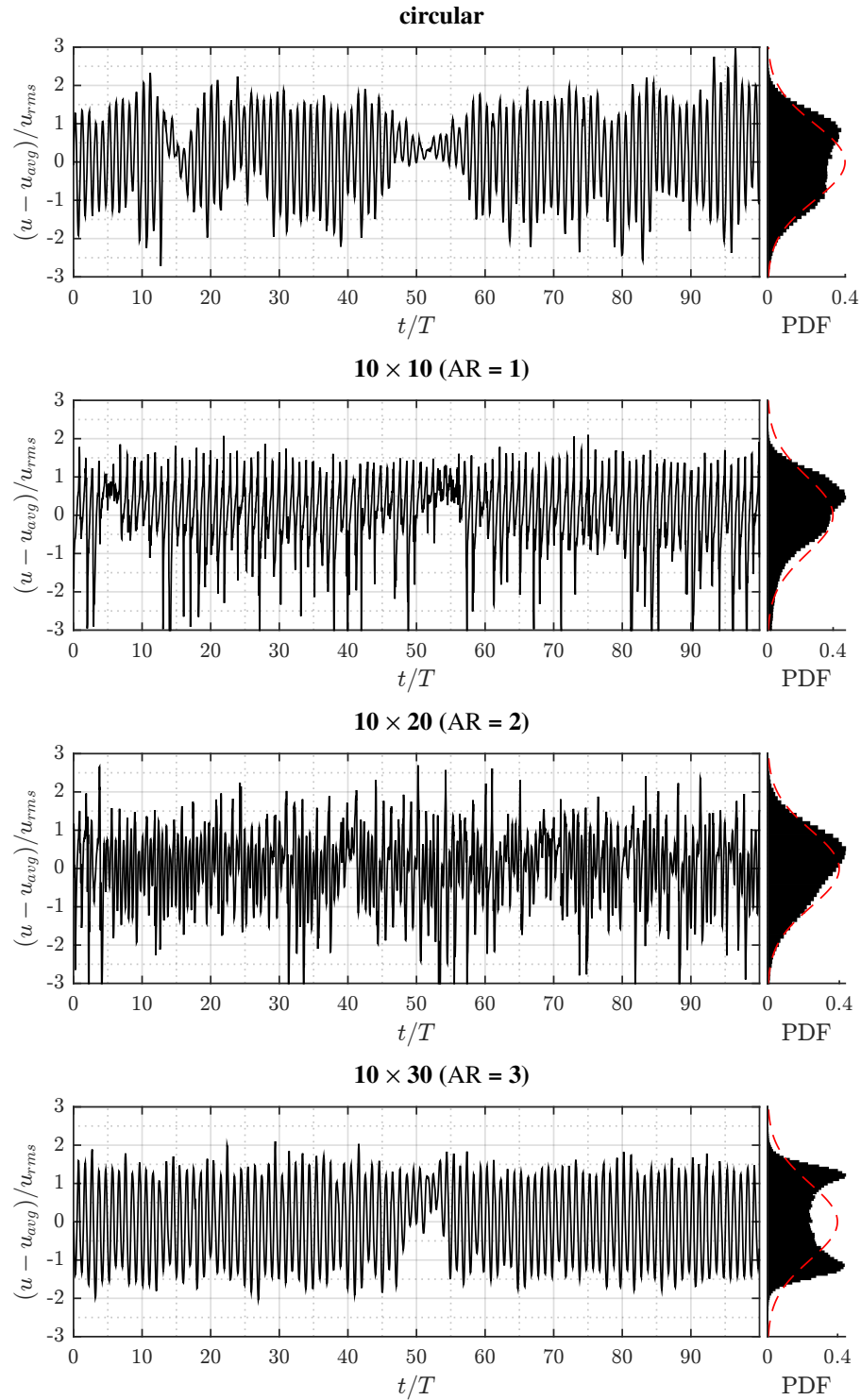


**Fig. 10** Samples of normalized flow velocity for the tested cross-sections near the expansion of the vortex for  $U_\infty = 20$  m/s, with the probability density functions (PDF) represented on the right (hatched line represents the normal distribution).

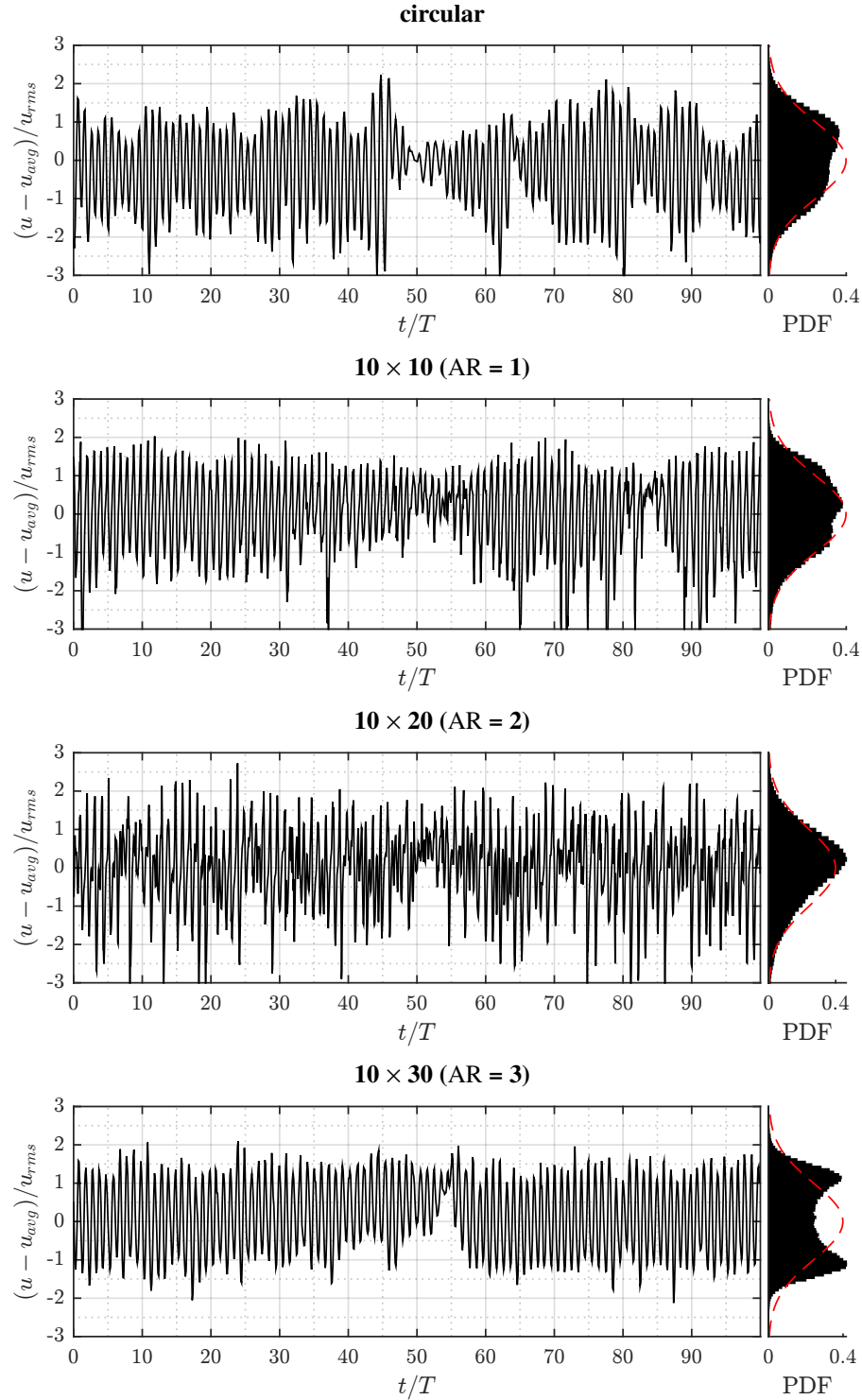


**Fig. 11** Same caption as Fig. 10, for  $U_\infty = 40$  m/s.

## B. Spanwise coherence length estimation

### 1. Coherence measurements

Hotwire measurements are performed at 10, 20 and 40 m/s, for different topologically equivalent locations in the XY plane, derived from flow streamwise velocity fields (also generated using hot wire anemometry). For the circular section,

only one position is selected, based on the consideration of Ribeiro [18]. Four points are tested for the rectangular sections:  $P_1$  (in the wake),  $P_2$  (in the position of maximum average velocity);  $P_3$  (at the upper limit of the mixing layer) and at  $P_4$  (at the zone of the expansion of the upper wall vortex). Measurements attributed to point  $P_4$  are considered the more reliable and representative of the pressure spanwise coherence, so are used here.

For the evaluation of the flow spanwise coherence, measurements with two hot wire probes are performed. The use of velocity signals has been reported capable of quantifying the coherence of surface pressure [18, 19], and consequently, of the lift. The flow velocity was recorded simultaneously at different spanwise positions using two 1D hot wire probes. The first probe is fixed at the middle span of the cylinder while the other is moving spanwise.

Acquisition time and frequency are of 30 seconds and 6.4 kHz. The coherence of the two signals  $u_a$  and  $u_b$  is calculated using the following definition:

$$\Gamma_{u,ab}(\omega) = \Gamma_u(\eta, \omega) = \frac{\text{real}(\bar{u}_a \bar{u}_b^*)}{\sqrt{\bar{u}_a^2} \sqrt{\bar{u}_b^2}} \quad (2)$$

where  $\omega$  is a frequency quantity (such as the Strouhal number or the frequency),  $\eta$  is the spanwise distance of the probes normalized by the diameter  $\eta = \Delta z/d$ ,  $\bar{u}_a$  and  $\bar{u}_b$  are the Fourier transforms of the fluctuations of each velocity signal, and the superscript \* indicates the complex conjugate. In order to obtain a more representative spectral distribution, the coherence calculations are based on averaged spectral density, using the same acquisition time and frequency as for the spectrum calculation.

## 2. Spanwise coherence length

The definition of the coherence length is based on a Gaussian model, as proposed by Casalino and Jacob [26]:

$$\Gamma_u(\eta, \omega) = \exp\left(-\frac{\eta^2}{2L_g(\omega)^2}\right) \quad (3)$$

where  $L_g$  is the Gaussian coherence length estimator (later on referred only as *coherence length*), normalized by the geometry height  $d$ , the same for all the geometries here.

A procedure for calculating the regression to obtain the Gaussian function and its associated  $L_g$  has been proposed. Description here will be limited to a single case, noting that it is similar for all the tested velocities and probe positions and that a complete description of the procedure and a discussion concerning these results are presented in [20]. Figure 12 illustrates some of the obtained results, considering point  $P_4$  for the rectangular sections, for flow at  $U_\infty = 20$  m/s.

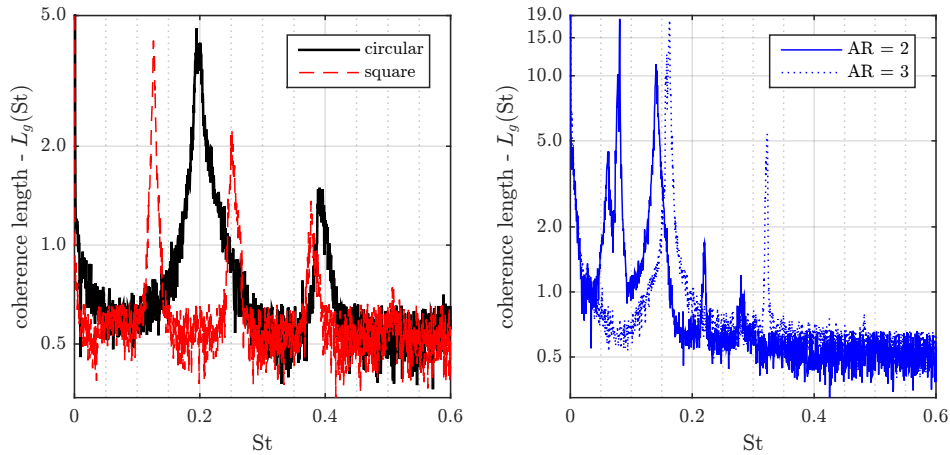


**Fig. 12** Samples of normalized coherence length for the tested cross-sections at  $P_4$  for  $U_\infty = 20$  m/s ( $Re = 13,333$ ) - for the circular section, the point is defined differently, see [20].

For the short sections (square and circular) the coherence length distribution is quite similar, with spread values around the fundamental mode and a clear mark of the first harmonic. At the vortex shedding frequency,  $L_g$  is of about 5 diameters, being slightly larger for the square section, as predicted by King and Pfizenmaier [5], who associate

this increase with the existence of a fixed separation point and with the source of a stronger sound emission. The rectangular sections of AR = 2 and AR = 3 present a poorer spectral distribution of  $L_g$ , and the later achieves about 20 diameters at  $St_{\text{peak}}$ . Considering this is a one-sided calculation, for a cylinder of  $\ell = 70d$ , the two flows are virtually two-dimensional.

The minimal threshold of about 0.6  $d$  is due to the used algorithm and to the limitations of the experimental setup. Indeed the first coupled hot-wire measurement is performed for  $\Delta z = 0.7d$ , so that coherence at smaller distances cannot be measured. Thus, those values are considered non physical. It may also be noticed that the curves are noisy. This is why a smoothing procedure is applied, presented on following section.

### 3. Continuous coherence length laws

**Modeling of coherence length peaks** Rather than selecting a single coherence length, or correcting only the principal mode ( $St_{\text{peak}}$ ) and its harmonics, and applying an arbitrary correction for the rest of the spectrum, as performed by Orselli et al. [30] and [24], the complete spectrum of coherence length is used to perform the sound emission magnitude correction in Section IV. The use of a regression function rather than interpolating the values for the frequencies of interest is justified by two reasons. Firstly, noisy character of the  $L_g$  values would lead to imprecise values, notably at the peaks. Secondly, the algorithm used for the calculation of  $L_g$  returns a minimum value of  $L_g \leq 0.6$  that is non-physical [20], of the same order that those obtained at the first point ( $\eta = 0.6$ ) used to measured the coherence length.

Visual analysis of Fig. 12 indicates that each peak and its associated slope may be represented by exponential laws, centered at the peak frequency. The following equation, based on asymmetric Laplacian, is introduced for a given peak  $i$ :

$$l_g^i(St) = m_i \exp\{-[(St - p_i)\psi_i s \kappa_i^s]^{\varepsilon_i}\} \quad (4)$$

where  $m_i$  is an amplitude parameter,  $\psi_i$  is a shape parameter defining the broadness of the peak (smaller the value of  $\psi_i$ , broader the peak),  $p_i$  is the location parameter indicating the peak location,  $\kappa_i$  is the asymmetry parameter (skew is positive for  $\kappa_i < 1$  and negative for  $\kappa_i > 1$ , symmetrical if unitary),  $s$  is the sign function of  $(St - p_i)$ , and  $\varepsilon_i$  is a decay parameter:  $\varepsilon_i = 1$  returns the Laplacian shape (pointed peak) while  $\varepsilon_i = 2$  returns a Gaussian-like decay. The final curve is the sum of each contribution, a continuous law of  $L_g$ :

$$L_g(St) = \sum_{i=1}^N l_g^i(St) \quad (5)$$

**Identification of the model parameters** Initially, the equation parameters  $p_i$  and  $m_i$  are set as the Strouhal and  $L_g$  values at each peak, respectively. The rest of the parameters are set arbitrarily as  $\psi_i = 10$ ,  $\kappa_i = 1$  and  $\varepsilon_i = 1$ , returning a symmetric Laplacian shape. With these values, a Nelder-Mead Simplex optimization [31] is performed individually for each peak, correcting the parameters of the function (for simplicity, the peak location  $p_i$  is fixed by hand). Only points at the frequency range delimited by the half distance between the neighboring peaks and that returned  $L_g$  above  $0.7d$  are considered. This restriction is in accordance with the limitation of the algorithm, evoked earlier, and of the experimental procedure, since the measurements start at that given spanwise distance so that no coherence length under that quantity is captured correctly.

The cost function is the square sum of the difference obtained between the model - Eq. (5) - and the measured coherence lengths with a penalization factor of 50 at the peak value. In order to obtain a corrected magnitude after summing all the contributions, the optimizations are performed sequentially, that is, the cost function considers the contribution of the previously optimized peaks. So, for the peak number  $k$ , we have:

$$\text{error}_k = \sum_{j \in \text{NB}} \left[ L_{g,j} - \sum_{i=1}^{k-1} l_g^i(St_j) \right]^2 + 49 \left[ L_{g,j_{\text{peak}}} - \sum_{i=1}^{k-1} l_g^i(p_k) \right]^2 \quad (6)$$

where NB represents the subs-set of indexes of frequencies that neighbor each peak and  $j_{\text{peak}}$  the index of the frequency that is closest to the max peak location  $p_k$ .

Also, in order to correctly reproduce the behavior close to null frequency, an artificial peak at  $St = 0.002$  is defined. For some cases, the threshold of minimum frequency is adapted to facilitate the convergence. A sample of the quality of the models is represented on Fig. 13. Better fit is observed for the circular cylinder, nevertheless the results are quite reasonable for the rectangular sections.

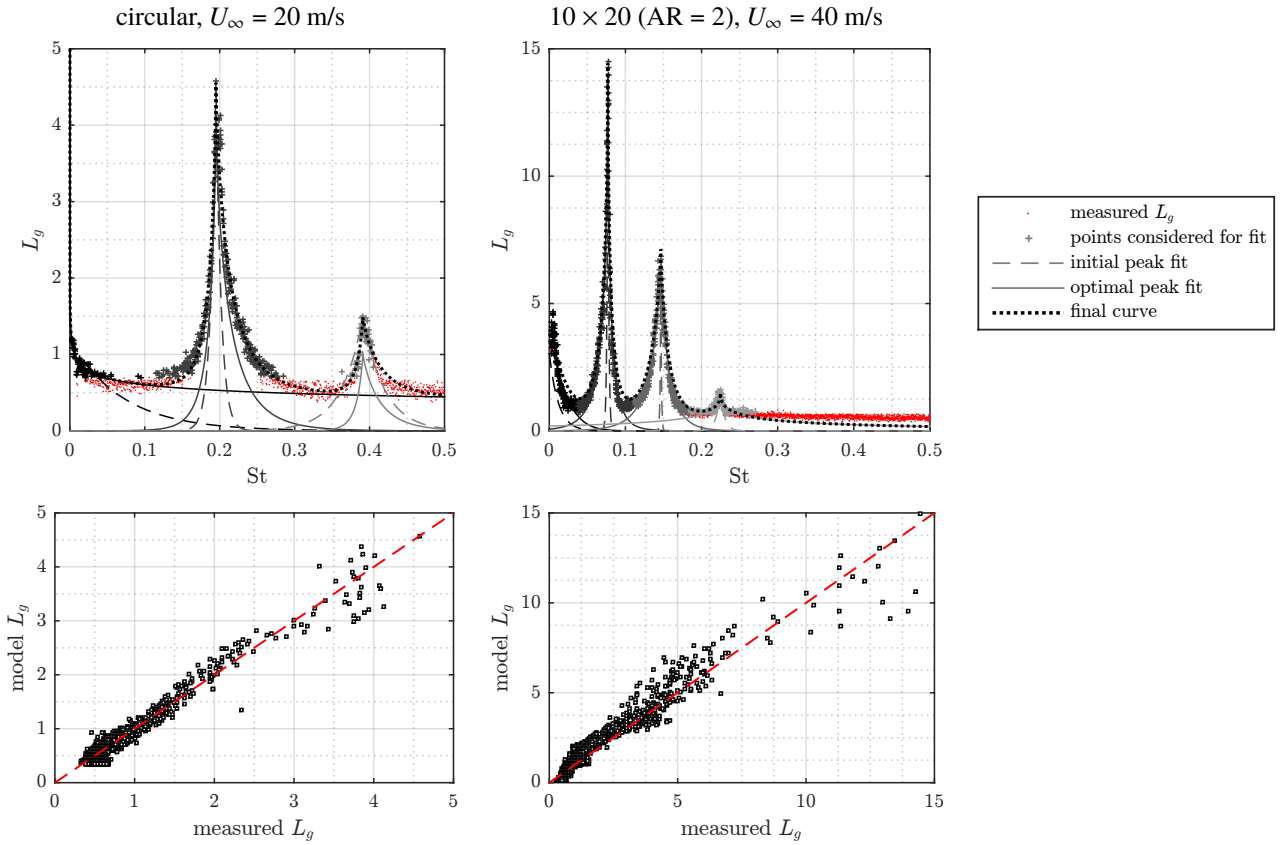


**Fig. 13** Examples of the fit for the circular (left) and rectangular section, AR = 2.0 (right).

**Influence of shape and velocity** A sample of the comparison of the obtained fits for all the tested section at different flow velocities is presented in Fig. 14. Remaining curves are presented on appendix.

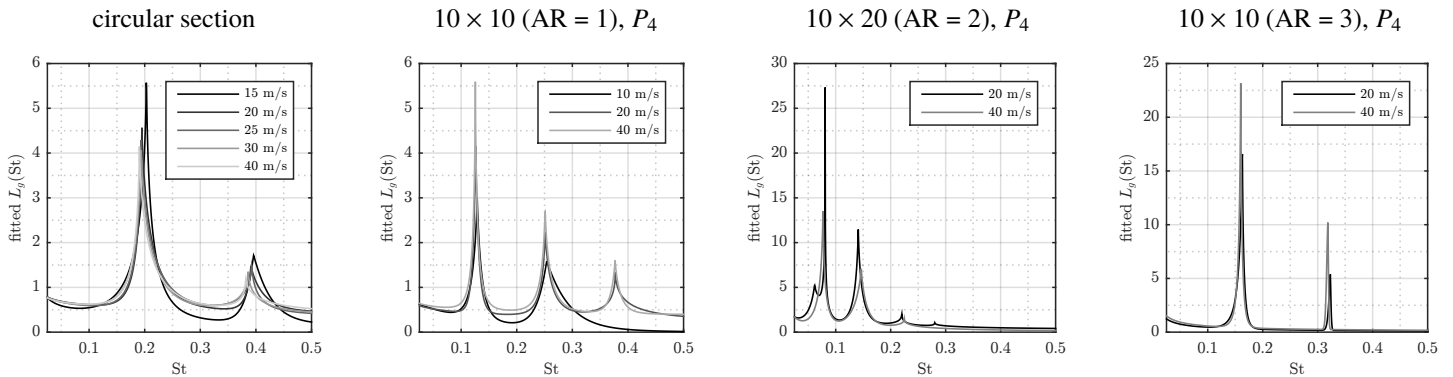


**Fig. 14** Regression laws  $L_g(St)$  for the the tested cross-sections, multiple velocities.

The results are extremely similar, even when modifying the flow velocity, specially in the peaks. This is in accordance with the small Reynolds number dependence at the studied regime noted by previous authors [32, 33] and reinforces the validity of using velocity data for such measurement [18, 19]. Nevertheless, the sectional position selected for the measurement has more influences the shape of the curve between the peaks. From the multiple points that are used to define the spanwise flow distribution for the rectangular sections (4 for square and 2 for AR = 2 and AR = 3), the relations obtained with  $P_4$  are selected for Section IV. Being the most distant from the surfaces, thus to the limitations

of the measuring procedure (difficulty to measure very small velocities) and less likely to be intrusive, those values are believed to be the most representative of the flow spanwise distribution.

Interesting point is that the second and third harmonics are barely present in the coherence length curves. That means that, once the fundamental mode and the first harmonic present in the flow aerodynamics, the following peaks may be seen as purely acoustic response of the flow, with a minimum correspondence to flow dynamics.

#### IV. How to close the body flow induced noise problem?

Working from the outside in, the influence of body shape and flow velocity on the acoustic field and on the spanwise coherence have been described. Further understanding of the influence of shape on the noise generation mechanism requires the analysis of the missing quantity in the Curle-Phillips formalism, that is the lift fluctuation, see Eq.(1). Ideally, the lift fluctuation should be measured in the same experimental conditions. A sectional lift could be extracted from an array of wall pressure probes. However, this misses the spanwise behavior and causes severe settling issues. In particular, each rod of cross section must be instrumented. Otherwise, the total lift may be obtained by aerodynamic balance, but then the spanwise distribution is integrated, and sectional behavior insight is prevented. Here, the sectional lift is educed by searching for it that, when joined to the measured spanwise coherence in Curle-Phillips formalism, would best approach the measured acoustic spectrum. This eduction is presented in the next subsection: first, a procedure to compute the acoustic spectrum from a given sectional lift signal is described, based on Seo & Moon [21] and Doolan [24]. Second, a sensitivity study is conducted in order to remove bias from parameter settings. Finally, the input lift coefficient that best fits the acoustic spectrum is identified, and the procedure is discussed in details with literature background.

##### A. Acoustic spectrum reproduction method

###### 1. Force model

Perfect sinusoidal signals are considered for the lift  $L$  and the drag  $D$  of a segment length  $L_s$ , with amplitudes defined by the RMS force coefficients  $C'_D$  and  $C'_L$ :

$$D = (C'_D \sqrt{2})(1/2 \rho U_\infty^2 d L_s) \sin(2\Omega_p t + \pi/2) \quad (7)$$

$$L = (C'_L \sqrt{2})(1/2 \rho U_\infty^2 d L_s) \sin(\Omega_p t) \quad (8)$$

where  $\Omega_p = 2\pi f_{\text{peak}}$  and  $t$  is the time. The modeled time sampling reproduces the duration and sampling used in the experiments.

###### 2. Peak broadening representation

For the association of the long-span behavior quantified experimentally with the sectional behavior, the procedure proposed by Doolan [24] is considered. Based on Curle's analogy, only the aerodynamic efforts are associated with the noise emission of the cylinder's section. The first step consists in applying a statistical correction for representing the natural random phasing that distributes the energy around the peak of each tone present in the sectional aerodynamic efforts (issued from a 2D simulation). The peak broadening is represented by an exponential decay, resulting in a modified 2D force vector  $F_T(t)$ , defined as:

$$F_T(t) \approx C \cos(\Omega t) \exp\left(-\sqrt{\frac{t}{4\tau_c}}\right) \quad (9)$$

where  $C$  is a real coefficient used to guarantee the energetic correspondence between original and modified force signals,  $\Omega$  represents the fundamental frequency at each dimension,  $t$  is the time and  $\tau_c$  is a turbulence time scale associated with the spreading of the peak. The turbulence time scale is represented as a multiple of the vortex shedding time scale, using the factor  $n_c$ , such as  $\tau_c = n_c / f_{\text{peak}}$ . As discussed by Doolan [24],  $n_c = 1.25T$  is the equivalent of a disturbance of duration of  $10 T$  as the ones observed in Section III.A.2.

### 3. Application of Curle's formula and long-span correction

After the peak broadening step, Curle's analogy is applied in the spectral domain in 2D compact formulation, that is, for the microphone at 90°:

$$\bar{P}(r, \omega) \approx \frac{i\omega}{4c} H_1^{(2)}\left(\frac{\omega r}{c}\right) \bar{L}(\omega) \quad (10)$$

where  $H_1^{(2)}$  is the Hankel function of second kind, order 1 and  $\bar{L}$  is the Fourier transform of the lift  $L$ , corrected using Eq. (7). See [34] for more details. Observer distance is of  $r = 1$  m, considering the wind-tunnel conditions.

Next step consists in correcting the sound level due to the spanwise extent of the cylinder using the procedure proposed by Seo and Moon [21]. For the extrapolation, the length  $L_s$ , taken as completely correlated, must be chosen. The total sound is then taken as a sum of the contribution of each segment, considering the dephasing present in the long-span using the coherence length  $L_c$ , a dimension associated with the correlation portion of the flow at each frequency. The following equation presents the correction level  $SPL_c$  that must be added to compensate the span effect on the spectrum obtained with the modified force (Eq. (9)):

$$SPL_c(\omega) = 10 \log_{10} \left\{ \sum_{i=1}^{N_s} \sum_{j=1}^{N_s} \exp \left[ -(i-j)^2 \left( \frac{L_s}{L_c(\omega)} \right)^2 \right] \right\} \quad (11)$$

where  $N_s$  is the number of segments, such as  $\ell = N_s L_s$ .

It does not account for the retarded time, so emission of very large cylinders may be overestimated. Also, the level correction accounting for the modification of the peak Strouhal values between the long cylinder and the experiment/simulation with short span cylinder, present in previous works [26, 30] and also used by Doolan [24], is not considered in this contribution.

Once all parameters are well posed, a sensitivity study, presented next, is performed in order to evaluate the influence of each parameter on the sound spectrum estimation, thus on the eduction of the RMS lift coefficient.

## B. Sensitivity study

### 1. Presentation

The influence of the number of segments  $N_s$ , the sectional aerodynamic efforts and the turbulence time scale  $\tau_c$ , represented by the number of periods of vortex shedding  $n_c$  ( $\tau_c = n_c / f_{\text{peak}}$ ), and the coherence length (calculated by the function  $L_c(\text{St})$ ) are tested for a fixed cylinder length of  $\ell = 70d$ . A simple factor is applied for each of these variables and the spectrum estimation is done. In order to vary the coherence length, the peak scaling parameter  $m_i$  in Eq. (4) is the only parameter that is modified.

When other parameters are tested, one takes:

- $N_s = 140$  (segment length of  $L_s = 0.5 d$ );
- $C'_L = C'_{L, \text{Norberg}} = 0.4728$ , issued from the empirical law presented by Norberg [19]);
- $C'_D = C'_L / 10$  as a first approximation;
- $n_c = 1.25$ ;
- $L_c = L_g$  as determined by Eq. (5) for the circular cylinder at  $U_\infty = 30$  m/s ( $\text{Re} = 20,000$ ).

### 2. Results

Spectral and peak behaviors are presented in Fig. 15.

In what concerns the number of segments/segment length, convergence is well defined. Values are extremely overestimated for long segments/small  $N_s$  once the calculation imply that a big subsection is completely in phase and producing noise corresponding to the sectional fluctuating coefficient. With the increase of  $N_s$ , levels are reduced for the complete spectrum. For the main peak, converged values are obtained after 10 segments. A change in the aerodynamic efforts represents a uniform offset of the sound levels for the complete spectrum; as expected the exponent for the fluctuating lift is 2. As proposed and illustrated by Doolan [24], the turbulence time scale  $\tau_c$  controls the sharpness of the spectral distribution, thus, is also highly influential on the peak level and shape of curve. The evolution of sound with the coherence length produces as well a global level offset, also presented by Seo and Moon [21] and the simplified equations, with an exponent of 1. The two highlighted exponents agree with the simplified model in Eq. (1). This result

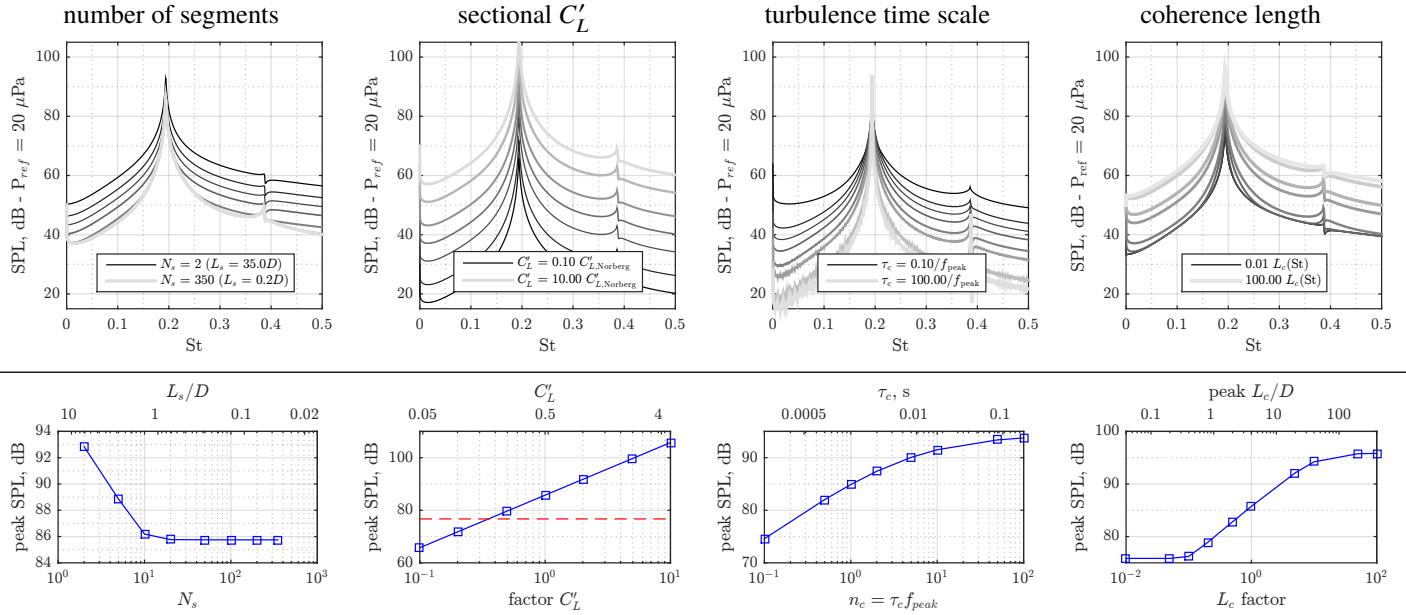


**Fig. 15 Sensibility study of the acoustic spectrum reproduction method. Influence on spectrum (top) and peak levels (bottom). Parameters are the number of segmentes  $N_s$ , the sectional fluctuating lift  $C'_L$ , the turbulence time scale  $\tau_c$  and the coherence length (function  $L_c(St)$  with different scale parameters); increase of the quantity is represented with the thickness of the line. Study is performed with data for the circular cylinder at  $Re = 20,000$ ; when not being analyzed, values are:  $N_s = 140$ ,  $C'_L = 0.4728$  [19],  $n_c = 1.25$  [24] and  $L_c(St) = L_g$  with coefficients as listed on Table 4. Hatched line represents the sound level obtained in the experiment.**

is consistent once the two procedures were derived from Curle's analogy and made the same assumptions (far-field, acoustically and geometrically compact source).

Based on the given analysis, the segment length is chosen as  $L_s = 0.5d$  ( $N_s = 140$ ). Although this spanwise distance was not evaluated in the coherence experiment, it is believed that for distance of half of that given length (comparing the extremities to the center of the segment) the coherence is close to one, independently of the frequency. In other words, the hypothesis is that a segment of that size is completely correlated in terms of fluctuating efforts and sound emission. The conversion factor based on the spanwise correlation, described by West & Apelt [35] and others, that links the sectional  $C'_L$  to the RMS lift coefficient of finite length cylinders serves as a quantitative criteria to justify this choice. This factor is calculated from the correlation of velocity signals [20] considering a segment of  $2d$ , imposing a symmetrical correlation distribution. Obtained results are higher than 0.9.

As intrinsically associated with the flow physics, later 3 varied parameters (actually, inputs) are case dependent and highly influential on the final spectra. Used values are presented next along the results of the application of the correction method.

### C. Lift eduction and artificial spectra

This procedure does not aim at estimating fluctuating efforts based on the acoustic emission. It is used as a complement of the analysis performed for the coherence length in the characterization of the cross-section influence on the flow and the acoustic emission. The analysis is here limited to 20 and 40 m/s, velocities that have been used for the spanwise coherence measurements for all the geometries.

Based on previous section, one takes  $L_s = 0.5d$ ,  $L_c = L_g(St)$  (measured). From Section III.A.2, an estimate of the turbulence characteristic time can be obtained, being the intermittent behavior on the velocity signals for the other sections quite similar to what is seen for the circular cylinder. Thus, the value  $n_c = 1.25$ , the as used by Doolan [24], what corresponds to a near-wall dislocation time of  $10T$  [19].  $C'_L$  is them educed by minimizing the error between artificially and measured acoustic spectra at each velocity for each cross section.

### 1. Definition of lift coefficient

There are two possibilities to define the lift coefficient in this case. Either the frontal surface is considered, that is, the reference area is defined as the product of the height  $d$  and the length of the prism  $\ell$ , or the streamwise surface is used,  $b \times \ell$  (for the circular and the square section both definitions return the same value since  $d = b$ ). They are calculated as follows:

$$C'_{L,d} = \frac{L'}{\frac{1}{2}\rho U_\infty^2 d\ell} \quad C'_{L,b} = \frac{L'}{\frac{1}{2}\rho U_\infty^2 b\ell} \quad (12)$$

where  $L'$  is the RMS lift. Each coefficient can be applied in a different context.  $C'_{L,d}$  may be directly compared to the drag and also considers the reference length for the wake. It can be considered as an engineering approach once the same analysis is performed for the whole group of geometries with a fixed reference, so the relation between the efforts can be direct among the set of different configurations, and interest quantities such as mechanical load or noise production are clearly stated. On the other hand,  $C'_{L,b}$  is not based on a fixed reference, and direct comparison of the fluctuating lift is not possible only regarding the coefficients. The interest remains in its association with the pressure fluctuation, since the effective surface that products the lift is taken as reference, thus it is called here a physics oriented coefficient. The authors recommend the lift coefficient to be explicitly defined in future publications, especially in the case of different sectional breadth.

Since the main objective in this work is the comparison of the sectional influence, first definition ( $C'_{L,d}$ ) is used, as can be in Eq. (7). When not explicitly defined,  $C'_L$  is used as a synonym of  $C'_{L,d}$ .

### 2. Searching for best acoustic spectrum fit

An optimization is done for the eduction of the forces RMS coefficients, applying the same techniques used for the determination of the coefficients of the  $L_g(\text{St})$  functions (Section III.B.3). For this case, there is no penalization for the peak and the error is the square value of the difference of the sound pressure levels in decibels. Ideally, analysis should be performed using two parameters:  $C'_L$  and  $C'_D$ . Due to its small influence on the final result and in employed Curle's formalism [34] for the microphone at  $90^\circ$ , the fluctuating drag coefficient is not considered as a variable in the optimization and its value is fixed as  $C'_D = C'_L/10$ .

For the calculation of the fit, different Strouhal ranges are considered, in order to favor the reproduction of different parts of the spectrum. Obtained artificial spectra are presented on Fig. 16 and 17 for the 4 tested sections, where each continuous lines corresponds to a different band considered in the error function. The lowest limit is associated to optimization accounting only for the fundamental peak ( $0.5 \text{ St}_{\text{peak}} < \text{St} < 1.5 \text{ St}_{\text{peak}}$ ). When a broader range is selected, a higher level appears such as to add energy to the first harmonic and neighboring frequencies. Maximum value for the optimal  $C'_L$  presented on figures correspond to the error function being calculated for  $0.5 \text{ St}_{\text{peak}} < \text{St} < 3.5 \text{ St}_{\text{peak}}$  (note that for the circular cylinder at  $U_\infty = 40 \text{ m/s}$ , all the measured sound spectrum above the peak is considered since the limit is  $\text{St} = 0.6$ ).

The current procedure reproduces extremely well the sound spectra found in the experiments, notably for the principal peak. This fact is fundamentally determined by the definition of  $C'_L$  that forces a good fit. However, the time decay and spectral correction levels defined by  $L_c(\text{St})$  and  $\tau_c$ , fixed in the optimization, are in accordance and may be considered a good estimation of the physics.

### 3. Discussion of the procedure and comparison to literature data

On Table 1, fluctuating lift and drag coefficients obtained in the optimization of the spectra are listed along with literature values. Since the hypothesis considered for the application of the correction algorithm is that the fundamental segment is small and completely correlated, the obtained RMS force coefficients correspond to sectional values.

The force coefficients are within the same order of what is available in the literature, however their magnitude is about 4 times smaller. Several factors could explain the discrepancy and are discussed next:

- From the purely acoustic point of view, **compactness and far-field hypothesis** present in theoretical formulation are not always respected in the current work, as depicted on Table 3, in appendix. Even if the natural tendency would be an increase of the level, what would result in a higher estimate of the RMS lift coefficient, it remains an unknown and may spoils the result. The differences in the retarded time of the segments are not accounted in the spanwise correction formulation proposed by Seo & Moon [21]. Applying this correction could represent a necessity of increased segment sound levels, that is, bigger  $C'_L$ , such as to reproduce the sound levels that are recorded, as can be deduced from formulation presented by Perot et al. [23] that considered this time delay.

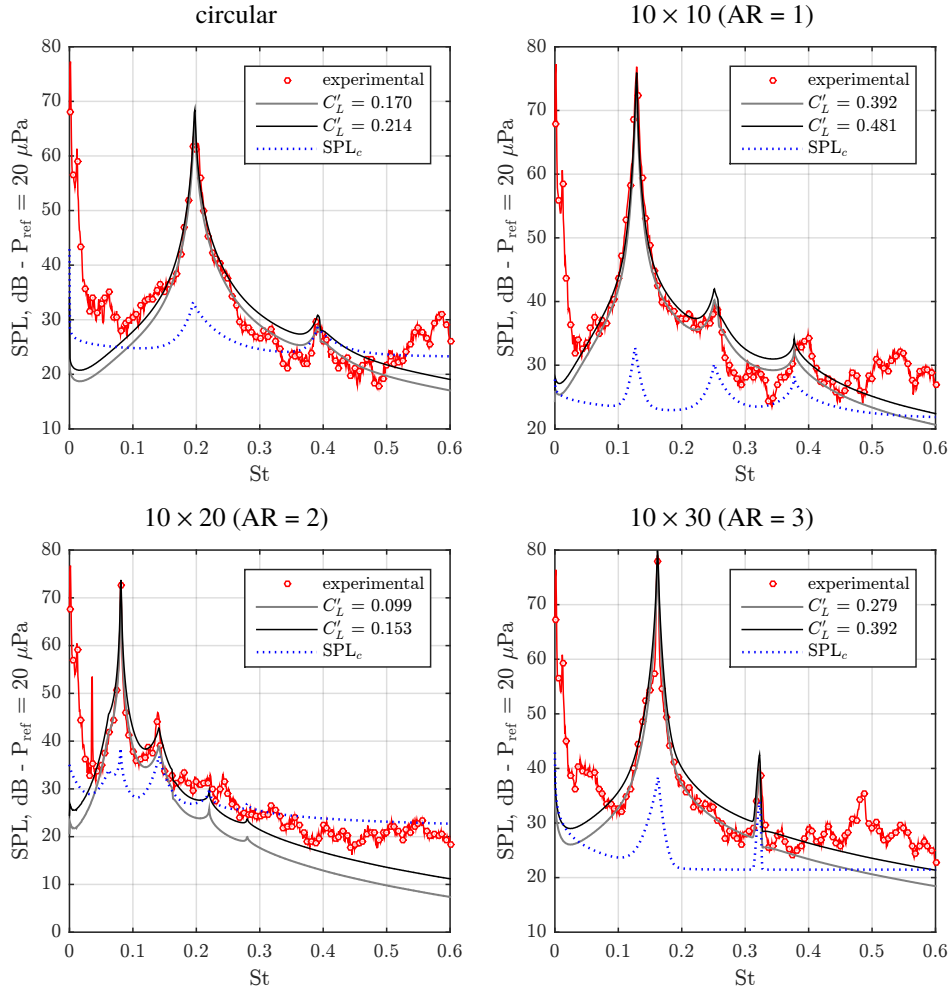


**Fig. 16** Experimental and optimal artificial sound spectra (solid lines) for  $U_\infty = 20$  m/s. The turbulent time scale is fixed, with  $n_c = 1.25$  (see section III.A.2), and  $L_c(St) = L_g$  is calculated with the coefficients as listed on Table 4. Circle markers are added to the experimental curve at every 12.5 Hz for visual aid, and the dotted line represents the spanwise correction level  $SPL_c$  (see Eq. (11)).

- The fluctuating lift for the circular section is explicitly given as sectional [19]. The authors could not find information about the rectangular sections that stated clearly to correspond to **sectional values**, represented by a measuring segment of reduced spanwise extension. Presented  $C'_L$  are the normalization of the efforts over the whole cylinder, that is, only a division of the total fluctuation lift by a reference surface ( $\ell \times d$  or  $\ell \times b$ ). In this case, the information available in the coherence length is actually present twice, and values of  $C'_L$  are miss-evaluated.
- There is a remarkable scatter in fluctuating coefficients data, especially scarce in experimental procedures. The fluctuating efforts are influenced by wind-tunnel conditions such as the incoming turbulence intensity [35, 41, 42]. Also, the tendency observed in the literature is to reinforce the 2D behavior of the flow by running simulations for very short cylinders and/or using end plates. Such choices artificially increase  $C'_L$ , described numerically [43, 44] and experimentally [45–47], where a length of at least  $20d$  is recommended for the circular section to prevent **confinement**. Considering that the coherence length is bigger for the other cross-sections studied in this work, it is implied that an even larger span is necessary to avoid the influence of the end conditions. Initially, Szepessy [46] attributed the increase of fluctuating lift to an increase of spanwise correlation. Current results [20] show that the spanwise correlation is rather similar to what is observed with end-plates when comparing to pressure coherence measurements performed by Casalino & Jacob [26] for the circular cylinder. In that sense, it is believed that the modification of the efforts due to end plates is more associated with the increase of strength of

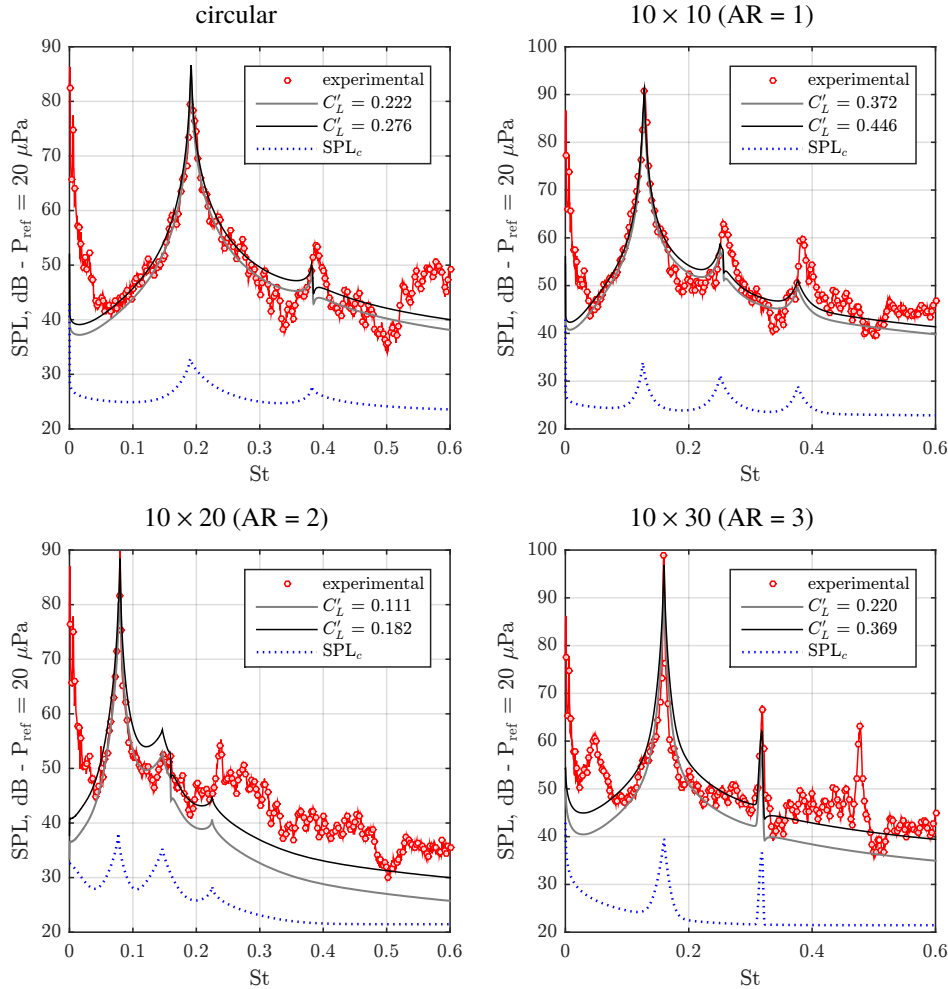


Fig. 17 Same caption as Fig. 16, for  $U_\infty = 40$  m/s.

the vortex and an increase in the perfect dephasing from the upper and lower parts of the flow, later proposed by Szepessy [48]. This could also justify why the sound levels obtained by Casalino & Jacob are similar to the current results with a cylinder that is of 1/3 of the current span. Even the results of Norberg [19], that clearly highlights the effects of end plates, may not be adapted for the present range ( $\ell/d = 26$  with supporting plates), as discussed in an earlier work [49].

- Values on the table for the rectangular sections are not at the same **Reynolds number**. However, the difference is considered to be small due to the observed independence of the flow around rectangular sections in this regime, as evoked previously in this document. This is noted for the square section in the review by Bai & Alam [33] and other works [42], and also evident in the values presented in the graph of  $C'_L$  versus the aspect ratio of the section at several Reynolds numbers, Fig. 20, that is discussed further.
- The **time scale parameter**  $\tau_c$  is grossly set and could not be determined with certainty for the different geometries in study. Also, the fact that the fit is good is not a sufficient criteria. In preliminary tests it was noted that multiple combinations of  $C'_L$  and  $n_c$  values can result in fits of similar quality. Further analysis was performed with the optimization of the  $n_c$  value considering a fixed  $C'_L$ , selected as the average value from the range listed on Table 1. Naturally the shape of the spectra is well respected, since it is the value that is minimized, however, results were unsuccessful with exaggerated values of  $n_c$  (from 5 to 170) and sound pressure levels at the vortex shedding frequency were consistently overestimated. Only reasonable result was obtained for the rectangle of AR = 3.0, with  $n_c$  between 1.7 and 7.3, but in accordance to the other results, peak level is overestimated of the order of 5 dB. Conclusion is that  $n_c = 1.25$  can be considered a representative value, however there is an intrinsically

**Table 1 Aerodynamic RMS lift coefficient in the literature and optimal values obtained from the fit of the sound spectra.**

section	Re, $10^3$		literature	optimal
circular	1.3	[36]	0.446	0.170-0.214
	2.7		0.484	0.222-0.276
$10 \times 10$ (AR = 1)	1.3	[37, 38]	1.15-1.71 <sup>†</sup>	0.392-0.481
	2.7		0.372-0.446	
$10 \times 20$ (AR = 2)	1.3	[16, 37, 39, 40]	0.83-1.36 <sup>†</sup>	0.099-0.153
	2.7		0.111-0.182	
$10 \times 30$ (AR = 3)	1.3	[16, 37, 39, 40]	0.35-0.57 <sup>†</sup>	0.279-0.392
	2.7		0.220-0.369	

<sup>†</sup>: literature values of fluctuating efforts for rectangular sections are not given for the section.

imprecision associated with this value, thus, an imprecision exists for deduced lift coefficient values.

- The effort model considered for Curle's analogy inside the algorithm are taken as **pure tones**. This means that all the energy is concentrated in  $f_{\text{peak}}$  and its first harmonic. Experimental and 3D simulations have a more distributed energy in the efforts spectra (for example, [50, 51] and [15, 42] for the circular and square cylinders, respectively), specially the neighborhood of the peaks. When compared to the tonal  $C'_L$  level, the only way of achieving the same magnitude at the peaks (which are the only points that influence the artificial sound spectra) would be to increase the total energy. Consequently, the optimal  $C'_L$  values are underestimated for not having a spectrally distributed energy and should be considered as pure tone analogous values.

## V. How Reynolds number, shape, sectional lift and spanwise topology combine

### A. Geometry ranking

The obtained hierarchies for flow and noise quantities are synthesized next, for the sound level (equally maintained for peak, band or overall), coherence length (considering the peak) and fluctuating lift (issued from the correction method, for a perfect sine wave):

$$\begin{aligned}
 \text{SPL:} & \quad \text{circular} < \text{AR} = 2.0 < \text{square} < \text{AR} = 3.0 \\
 L_g: & \quad \text{circular} \lesssim \text{square} < \text{AR} = 2.0 \approx \text{AR} = 3.0 \\
 C'_L: & \quad \text{AR} = 2.0 < \text{circular} < \text{AR} = 3.0 < \text{square}
 \end{aligned}$$

It appears that there is no direct association between the 3 hierarchies, although the extrema (circular and AR = 3) are reproduced in both SPL and  $L_g$ . It must be recalled that the time scale  $\tau_c$  is considered the same for all cases.

As predicted by King & Pfizenmaier [5], the square prism has a coherence length larger than the circular section. However, the difference in the sound emission is also due to a modification of the wall pressure fluctuations, represented by the increase of the RMS lift coefficient. Current results reinforce partially the statement of Iglesias [7], that implied that the difference in sound emission of the rectangular sections comes from an increase of the coherence length. Even though there is a prominent variation of the  $L_g$ , it is as important as the difference of the  $C'_L$  when square and other rectangular sections are compared. A computation of the contribution of each variable based on the model in Eq. (1) was tried. The results were not capable to fully described the difference noted in the wind-tunnel, and may indicate that the model is too reducing or that some of the hypothesis may not be fully respected.

## B. Sectional lift fluctuations and spanwise coherence length

It is possible to conceive that the sectional lift coefficient grows in the inverse direction of the coherence. A relationship is presented in Fig. 18, considering the peak coherence length returned from the continuous coherence length functions and the center of the range of fluctuating lift coefficients issued from the optimizations of spectra, along with a regression law. The correction and fitting procedure is also performed for the other velocities tested for the circular section that were not discussed in the previous session ( $U_\infty = 15, 25$  and  $30$  m/s). Error bars are set as  $0.7d$  for the coherence length and the limits for the  $C'_{L,b}$ . Note that the used coefficients are based on the breadth of the geometry.

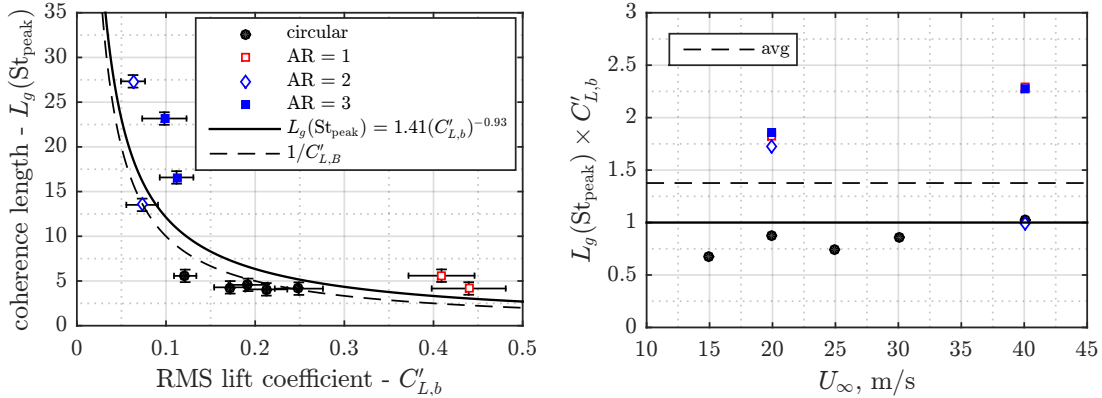


**Fig. 18** Comparison of the coherence length at the peak frequency  $L_g(St_{peak})$  and the  $b$  based RMS lift coefficient  $C'_{L,b}$  (left) and the evolution of their product with the flow speed (right).

Obtained least-squares fit regression laws (determination coefficient of  $R^2 = 0.63$ ) are the following:

$$L_g(St_{peak}) = 1.41(C'_{L,b})^{-0.93} \quad C'_{L,b} = 0.64 L_g(St_{peak})^{-0.68} \quad (13)$$

Since the method used to obtain the estimations of the fluctuating lift coefficient involves the coherence length as an input, the result may be biased. Even so, and despite the impreciseness in the determination of  $C'_L$ , this result seems to be physically consistent. That is: a cross-section with an important pressure fluctuation (large  $C'_{L,b}$ ) will most likely generate a spanwise flow distribution that is as well uncorrelated (small  $L_g$ ). The same comparison is not successful when the engineering coefficient  $C'_{L,d}$  is considered, since the lift is directly modified by the available streamwise surface and does not correspond only to the vortex strength and associated pressure fluctuations.

Even if preliminary, a link between the sectional and axial behavior has thus been unearthed. Further analysis concerning the shape influence on the sectional behavior are presented next.

## C. Further analysis of the sectional behavior

### 1. Reynolds number dependence for the circular cylinder

Figure 19 presents the evolution with the Reynolds number of the observed estimation of  $C'_L$  for the circular cylinder and literature values; a length of  $\ell/d = 0$  indicates a sectional coefficient, obtained either from the movement of a short segment or from wall pressure captors distributed around the section. Current results are represented by markers at the limits of the range of optimal values, illustrated on Fig. 16 and 17, and lines that connect the center of those ranges. Coefficients deduced from the application of Eq. (1) (without the use of the near wake correction term) with the quantities associated to the vortex shedding frequencies are as well presented, that is:

$$C_L'^2 = \frac{\bar{P}_{peak}^2 16c^2 r^2}{\rho^2 U_\infty^6 St_{peak}^2 \ell L_g(St_{peak}) d} = \frac{\bar{P}_{peak}^2 16M^2}{\rho^2 U_\infty^4 St_{peak}^2 \ell L_g(St_{peak}) d} r^2 \quad (14)$$

On Fig. 19 current values are about 3 times smaller than what is observed in the literature. Many factors influence that difference, as listed on section IV.C.3. As stated earlier, the objective of the present lift reduction is not to measure the lift coefficient from the noise emission, but rather compare between different cross sections the perfectly sinusoidal

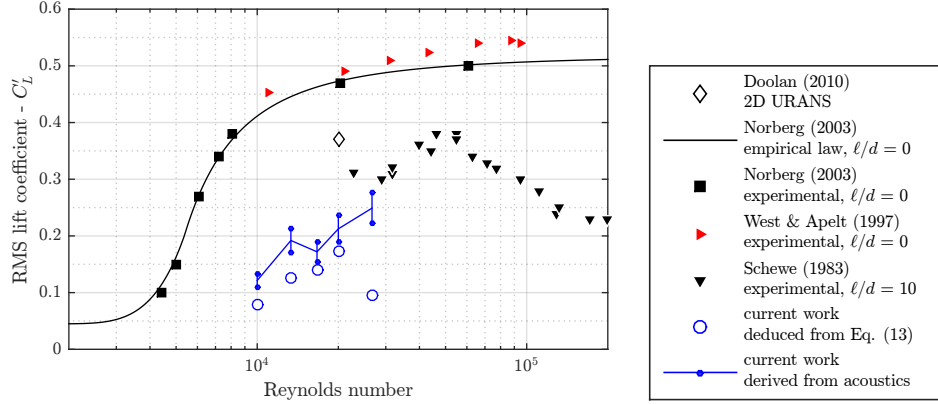


**Fig. 19 Comparison of currently estimated circular cylinder RMS lift coefficients with literature values at different Reynolds numbers [19, 24, 35, 50].**

lift and drag fluctuations that would generate an equivalent sound emission. Even if the amplitudes are underestimated, the increase of  $C'_L$  with the Reynolds number present in published values is well reproduced in current results, what can be directly associated with the reduction of coherence length noted in [20], as discussed in the previous section (V.A). The fact that the values derived from Eq. (1) by Fujita [10] are smaller is attributed to the absence of the correction associated with the distribution of the energy around the spectra peak, what is accounted with the  $\tau_c$  time scale. Furthermore, we may conclude that if the spanwise energy distribution is removed (it is going to be applied later in the correction), the corresponding  $C'_L$  values that would produce the same acoustic energy are significantly smaller.

In that sense, the success of the first test case presented by Doolan [24] with an overestimated  $C'_L$  is attributed to performing the validation with an also overestimated sound emission data from Casalino & Jacob [26]. Their sound pressure levels are quite similar to the new results introduced here, Fig. 4, even if the current cylinder is more than 3 times longer and flow velocity is higher. This similarity is believed to be the effect of the end plates. The used coherence length of  $5d$  is also overestimated, as discussed in [20].

## 2. Influence of aspect ratio for rectangular cylinders

**General trends** For the rectangular section, the literature and current  $C'_L$  values are presented in Fig. 20. Low (left) and high (right) Reynolds number values are considered. Similarly to what is employed on previous plots, current results are represented by markers at the optimal values issued from the optimization and lines connect the central position for each aspect ratio. Note that only one experimental study could be found and that all the cited works use very small extent in the spanwise direction.

The evolution of the fluctuating lift consists of an increase until a maximum  $C'_L$  at around  $AR = 0.6$ , and a decrease for longer geometries. The "golden ratio" of 0.6 has been discussed in several previous works, notably the references of Fig. 20. This bi-phased behavior of the  $C'_L \times AR$  curve is common for all geometries and is discussed in another paper presented by the authors in the same conference [13], that discussed the flow around other shapes such as ellipses and triangles. After the breadth has a significant number of diameters, there is a slight recovery, in a somehow oscillating curve that may be associated with the position where the vortex are generated. Similar shape is present in all plots, except for low Reynolds number when considering the breadth as the reference length. This traduces the fact that at lower Reynolds number, the available surface is a main factor in the creation of the lift fluctuation and the pressure tends to infinity with the decrease of  $b$ . The behavior is different at high Reynolds number, where the short sections are associated with small  $C'_{L,b}$ . This may be due to a loss of coherence associated with the small available surface in the streamwise direction. Even if the detachment point is fixed, the vorticity generating region is rather small and more subjected to vortex dislocations and three dimensional developments. This correlates to the discussion about the inverse relationship that is noted between the sectional efforts and the spanwise coherence.

**Magnitudes** It may be noted that the educed values for  $C'_L$  are close to literature for the rectangular section of  $AR = 3$ , what may be related to two factors. First, the coherence length is really high, what represents an almost two-dimensional flow. In this case, a true sectional  $C'_L$ , measured for a reduced section, would be close to the same as a total cylinder

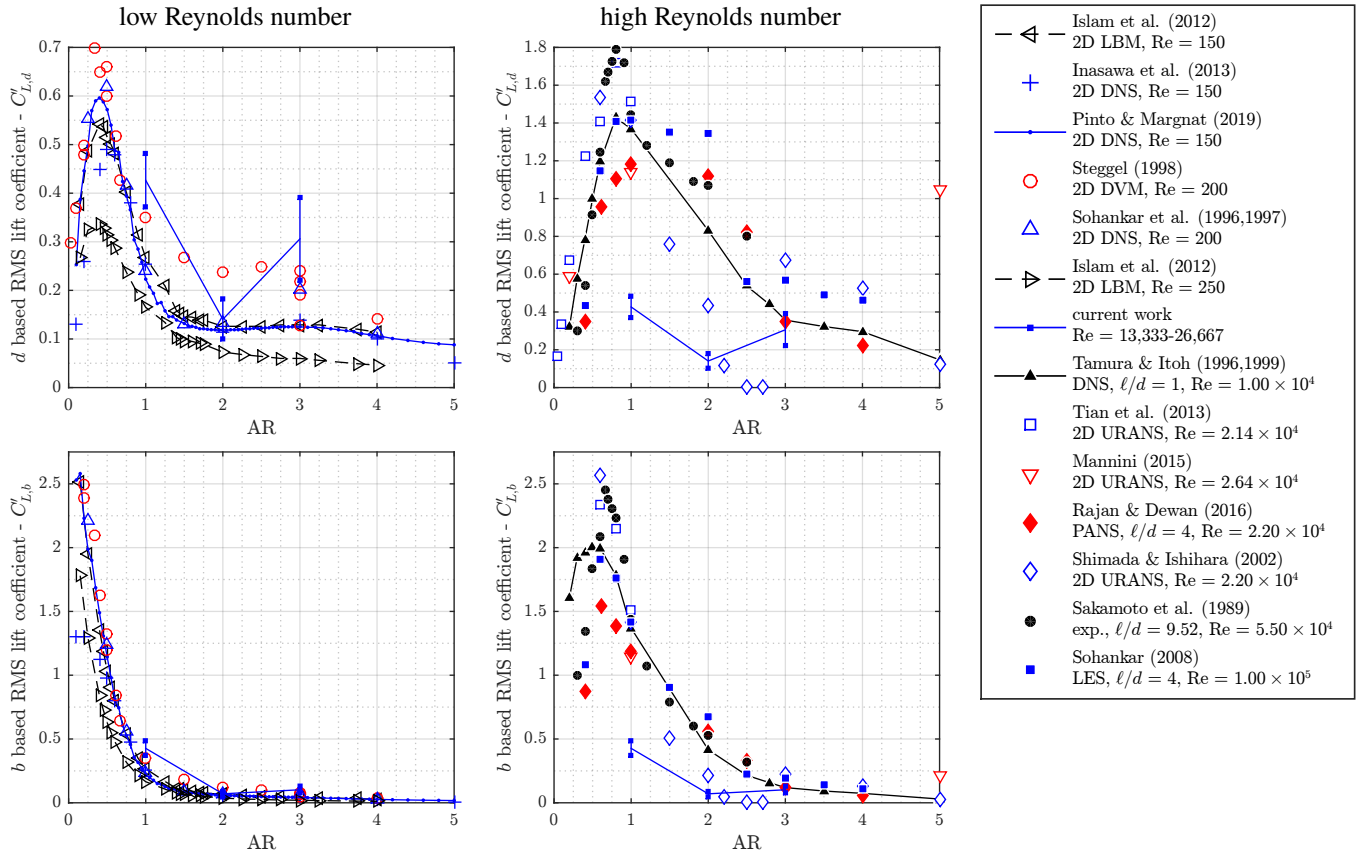


**Fig. 20 Comparison of currently estimated rectangular cylinder  $d$  based and  $b$  based RMS lift coefficients with literature values at low [12, 13, 52–55] and high Reynolds numbers [16, 17, 37, 39, 40, 56–58].**

force coefficient normalized by  $\ell$ . Secondly, as can be noted on the velocity signals in Fig. 10 and 11, the fluctuating lift for that geometry is more of a pure tone, so that an estimation of the perfect sine wave lift and drag in the statistical correction is close to the reality of the flow.

It can also be inferred that, per available lifting surface, the longer geometries undergo less pressure fluctuations, as presented on the graph for  $C'_{L,b}$ . However, that effect is surpassed by the increase of the available surface and of the coherence, thus giving an increase of the sound emission, exactly in the opposite direction of what is noted on the sectional behavior. We may also imply from current results that the behavior noted in the OASPL vs AR graph (Fig. 9) is not due to the modification of the Strouhal, as discussed by Octavianty et al. [9], but rather to a combined increase of  $L_g$  and  $C'_{L,d}$ . Naturally, all three quantities are intrinsically related and a clear description of their relationship should need a greater database and a refined physical modeling.

Another important conclusion concerns the fact that the obtained  $C'_L$  are relatively close to those obtained by low Reynolds number simulations. The current procedure implies that the transition from a short to long geometry is possible, meaning that an homogeneity in the axial dimension is assumed. Also, the correction of the tonal efforts implies that most of the low amplitude features of the aerodynamic efforts spectra can be neglected and that the peak neighborhood is correctly represented by an exponential decay. In short, given these hypotheses and current results, the procedure allows a connection between the 2D low Reynolds number (tonal) to 3D flows: the transition from low to high Reynolds number is condensed in the  $\tau_c$  correction, and the transition from 2D to 3D in the coherence length. This is particularly consistent in the case of rectangular sections, where the flow is rather Reynolds number independent for an important range of velocities.

## VI. Conclusions

The influence of the geometry and of the Reynolds number in the noise production of prismatic body flows has been investigated experimentally. Sound levels and spanwise coherence lengths were measured for circular and rectangular cylinders. The statistical analysis and correction procedures for the spanwise influence on cylinder's airframe noise proposed by several authors [21, 23, 24, 26] is successfully applied to different cross sections, leading to estimations of the RMS lift coefficient considering the aerodynamic effort as two perfect sinusoidal waves.

One interesting result is that the sound production hierarchy between the geometries (circular  $<$  AR = 2  $<$  square  $<$  AR = 3) is held for all the Reynolds numbers tested in this experiment. One logical conclusion would be that, for a given velocity range where there is not a known transition, as the one used in this work, there is, a priori, no necessity to perform a Reynolds dependency study when confronting sound production of different geometries.

While the use of end-plates is highly advocated for the reduction of end conditions interference in flow, its influence is responsible for forced increase of the aerodynamic efforts. In the case of long cylinders ( $\ell/d > 15$ ), the authors believe that end-plates are more influential than the presence of open ends and must be avoided once they create a different flow and a more important sound emission.

Despite the good fit that is observed in the modeled sound spectra, the educed fluctuating lift coefficients are smaller than what is present in the literature. Although that behavior was expected due to the simplification of the efforts into clean sinusoids and the difficulty associated with measuring fluctuating aerodynamic efforts, it may indicate a deficiency in the applied technique. In all likelihood, the not so strict respect of the far-field and compact conditions would not produce such important errors. Furthermore, the spanwise statistical correction method used in this work is a reformulation of the classical equations derived by Curle [1] and Phillips [2]. To the authors knowledge, until this day no simultaneous measurement of all the ingredients ( $C'_L$ , spanwise coherence and sound emission) has been performed. It is thus necessary, as hoped by Lighthill [11], to perform a systematic test of such physical and mathematical reasoning. The work of Leehey & Hanson [59] is the only one the authors could find that performed something similar to that. However they were using a vibrating cylinder at a low Reynolds number range (4000 to 6450) and performed the calculations with the correlation length, that is found to be lower than the coherence length [20]. Similarly, the validity of the procedure to correct the sound emission by sum of segments, that was used to educe the sectional lift in this article, has to be further checked both theoretically and experimentally, as far as fair comparison between shapes is targeted.

As implied by previous works [5, 7], sharp-edged sections are more coherent. However, the difference in coherence alone does not justify the offset found in the acoustical signature of each prism. Performed analysis shows that they are not only more coherent but also have greater sectional RMS lift coefficient. Current results also indicate that the spanwise coherence length is inversely proportional to the fluctuating lift, such that the acoustic emission is more influenced by the modifications of the pressure fluctuations and the available surface than by the spanwise characteristic of the flow, not forgetting that the latter is a result of the first two.

This correlates to an energetic point of view interpretation of the spanwise direction as a path for the distribution of the wake energy, and that each shape follows the same set of flow transitions (respectively wake, shear layer and boundary layer [60]). In this conception, the geometry of prismatic bluff bodies acts analogously to a boundary condition or forcing term that advances or delays where, in the Reynolds number scale, the changes in the flow structure are going to take place. For a fixed velocity, each cross-section places the flow at a different position of that scale, what must be also finer assessed considering the instability formalism. Hence, as discussed in a previous work [20], the authors believe that the analysis of the geometry influence in the flow may also be seen as a virtual modification of the Reynolds number. For instance, in this experimental campaign, the AR = 3 rectangular cylinder presented characteristics that are equally noted in the flow around the circular section at lower Reynolds number: sharp tone in the acoustical signature, high coherence length. In this sense, the description of sectional flows, in both low and high Reynolds, are seen as a fruitful path into the better understanding of the shape influence on bluff body flows and aeroacoustic emission. Once fine descriptions of canonical geometries such as the circular cylinder and, in a smaller scale, the square prism are established, more attention should be given to the geometry dependence.

In terms of strategies of reducing airframe noise and structural vibrations, current results lead to the following 2-step proposition: (i) increase the breadth of the cross-section such as to reduce the flow fluctuations and the strength of the vortex (decrease of  $C'_{L,b}$ , as is observed in low Reynolds 2D simulation); and (ii) add flow spanwise decorrelation devices, such as surface protrusions and shrouds [61], in order to compensate for the increase of the coherence. Since the tonal trait will be increased, this may not be fully advantageous, also due to the increase of available surface (illustrated by the curve of  $C'_{L,d}$ ). This logic must be seen as a general direction rather than a guaranteed procedure.

## Appendix

### A. Experimental conditions

Table 2 lists the range of velocities tested in this work and the corresponding Reynolds and Mach numbers.

**Table 2** Experimental conditions.

$U_\infty$ , m/s	10	15	20	25	30	40
Re	6,667	10,000	13,333	16,667	20,000	26,667
Mach	0.03	0.04	0.06	0.07	0.09	0.12

### B. One-third octave levels

Obtained one-third octave levels are presented on Fig. 21 for the central microphone ( $\theta = 90^\circ$ ), considering all the tested sections at  $U_\infty = 30$  m/s ( $Re = 20,000$ ). Levels obtained for the circular cylinder are compared to literature values.

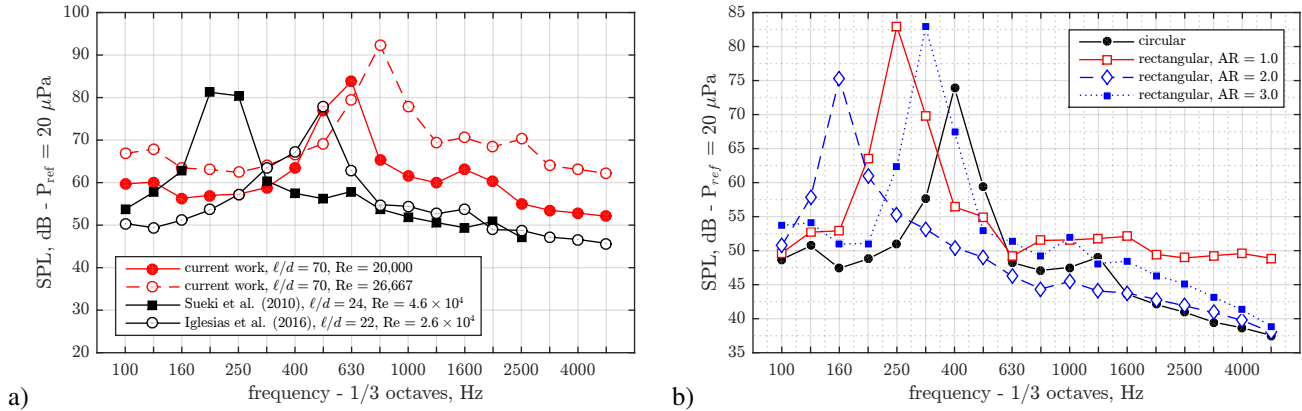


**Fig. 21** 1/3 of octave sound pressure level (SPL) for the circular cylinder (a) and for all tested sections (b) ( $Re = 20,000$ ,  $M = 0.09$ ). Comparison with data from the literature [7, 27].

### C. Peak frequencies and levels database

Measured vortex shedding frequencies, wavelengths and corresponding sound levels are listed on Table 3 for all tested cross-sections and flow velocities. Three procedures for quantifying the noise are used to allow the comparison of the sound production between the sections and also available data in the literature: a) the sound pressure level at the tone frequency (PSPL); b) the overall sound pressure level (OASPL), calculated by the integral of the power density for the tested range,  $f \in [0, 6400]$  Hz; and c) the band sound pressure level (BSPL) calculated by the integral of the sound pressure density over the frequency range whose lower and upper limits correspond to SPL levels that are some decibels down from the peak SPL value, as performed by Hutcheson and Brooks [29] with -10 dB and Haramoto et al. [25] with -3 dB. Only the first quantity for -10 dB is presented in the appendix.

Considering the vortex shedding frequency and its associated wavelength, the microphone array is not in far-field ( $r > \lambda$ ) for most of the measurements. The compactness of the cylinder ( $\ell < \lambda$ ) is obtained for most of the measurements. The near field contribution proposed by Fujita [10], Eq. (1), is also listed.

**Table 3 Peak frequencies and pressure levels.**

	$U_\infty$ ,	$St_{\text{peak}}$	$f_{\text{peak}}$ , Hz	acoustic wave length		PSPL <sup>†</sup> , dB*	OASPL <sup>‡</sup> , dB*	BSPL <sup>§</sup> , dB*	near field <sup>¶</sup> , dB*	
	m/s			$\lambda$ , m	$r/\lambda > 1$					$\ell/\lambda < 1$
circular	10	0.208	208	1.64		✓	43.9	73.2	46.1	0.28
	15	0.204	306	1.11		✓	55.1	77.2	62.8	0.13
	20	0.197	394	0.86	✓	✓	63.8	80.4	73.5	0.08
	25	0.194	486	0.70	✓	✓	72.8	85.7	82.2	0.05
	30	0.193	578	0.59	✓		74.2	88.5	84.1	0.04
	40	0.191	766	0.44	✓		80.4	94.4	91.9	0.02
rectangular, AR = 1	10	0.128	128	2.65		✓	62.1	73.5	65.9	0.71
	15	0.129	194	1.76		✓	68.7	78.2	74.1	0.33
	20	0.129	258	1.32		✓	76.9	84.7	82.7	0.19
	25	0.129	323	1.05		✓	79.4	88.5	86.3	0.12
	30	0.129	386	0.88	✓	✓	84.3	93.2	91.8	0.08
	40	0.129	513	0.66	✓		90.8	100.5	99.6	0.05
rectangular, AR = 2	10	0.089	89	3.82		✓	47.4	72.9	50.7	1.36
	15	0.082	123	2.75		✓	68.2	77.2	70.4	0.76
	20	0.081	163	2.09		✓	72.6	80.5	75.0	0.46
	25	0.080	200	1.70		✓	71.8	84.4	79.4	0.31
	30	0.080	241	1.41		✓	85.9	91.2	89.3	0.21
	40	0.080	319	1.07		✓	89.8	95.7	93.8	0.12
rectangular, AR = 3	10	0.167	167	2.03		✓	57.8	73.9	59.7	0.43
	15	0.164	245	1.39		✓	73.6	79.3	76.3	0.21
	20	0.162	323	1.05		✓	79.0	84.4	82.6	0.12
	25	0.161	403	0.84	✓	✓	86.1	91.3	90.4	0.08
	30	0.160	480	0.71	✓	✓	92.7	97.3	96.8	0.05
	40	0.160	639	0.53	✓		99.0	104.5	104.2	0.03

\*:  $P_{\text{ref}} = 20\mu\text{Pa}$

†: sound pressure level at the tone frequency

‡: overall sound pressure level, integral of power spectral density  $f \in [0, 6400]$  Hz

§: band sound pressure level, integral of power spectral density over the frequency range whose lower and upper limits correspond to peak SPL - 10 dB [29]

¶: near field contribution [10]:  $10 \log_{10} [1 + (\lambda/2\pi r^2)]$

#### D. Coherence length functions

Coefficients for the continuous coherence length functions, presented on Section III.B.3, are listed on Tables 4 and 5, for the circular and rectangular cross-sections, respectively. First peak ( $i = 1$ ) corresponds to the artificial peak added at  $St = 0.005$  used to account for the coherence at very-low/null frequency. Corresponding plots are given on Fig. 14, 22 and 23.

**Table 4 Coefficients for the coherence function  $L_g(St)$ , circular section.**

$i$	1	2	3	4	5	6	
15 m/s	$m_i$	$6.04 \times 10^{12}$	5.697	1.504	-	-	-
	$\kappa_i$	$6.61 \times 10^{47}$	1.163	0.690	-	-	-
	$\psi_i$	$2.35 \times 10^{49}$	82.958	45.828	-	-	-
	$\varepsilon_i$	0.015	0.636	1.051	-	-	-
	$p_i$	0.000	0.203	0.396	-	-	-
20 m/s	$m_i$	$8.80 \times 10^5$	4.042	1.015	-	-	-
	$\kappa_i$	$3.57 \times 10^{43}$	0.694	0.611	-	-	-
	$\psi_i$	$6.26 \times 10^{44}$	77.553	69.643	-	-	-
	$\varepsilon_i$	0.013	0.763	0.874	-	-	-
	$p_i$	0.000	0.195	0.391	-	-	-
25 m/s	$m_i$	$5.26 \times 10^7$	3.828	1.112	-	-	-
	$\kappa_i$	$1.69 \times 10^{50}$	0.679	1.098	-	-	-
	$\psi_i$	$1.48 \times 10^{51}$	72.584	74.403	-	-	-
	$\varepsilon_i$	0.013	0.718	0.623	-	-	-
	$p_i$	0.000	0.193	0.393	-	-	-
30 m/s	$m_i$	$1.81 \times 10^7$	3.626	0.956	-	-	-
	$\kappa_i$	$2.83 \times 10^{50}$	0.804	0.942	-	-	-
	$\psi_i$	$3.59 \times 10^{52}$	65.937	65.578	-	-	-
	$\varepsilon_i$	0.012	0.749	0.583	-	-	-
	$p_i$	0.000	0.193	0.386	-	-	-
40 m/s	$m_i$	$7.90 \times 10^6$	3.624	0.741	-	-	-
	$\kappa_i$	$7.55 \times 10^{54}$	0.709	0.560	-	-	-
	$\psi_i$	$2.39 \times 10^{55}$	73.514	65.187	-	-	-
	$\varepsilon_i$	0.011	0.688	0.543	-	-	-
	$p_i$	0.000	0.190	0.382	-	-	-

### Acknowledgments

The PhD funding of the first author was provided by the Ministère de l'Enseignement Supérieur et de la Recherche (MESR, french Ministry of Higher Education and Research), which is greatly appreciated. The authors are also grateful to Janick Laumonier, Laurent Philippon and Pascal Biaïis for their fundamental contributions to the experiments performed in this work.

### References

- [1] Curle, N., "The influence of solid boundaries upon aerodynamic sound," *Proceedings of the Royal Society of London A: Mathematical, Physical and Engineering Sciences*, Vol. 231, No. 1187, 1955, pp. 505–514. doi:10.1098/rspa.1955.0191, URL <http://rspa.royalsocietypublishing.org/content/231/1187/505>.
- [2] Phillips, O. M., "The intensity of Aeolian tones," *Journal of Fluid Mechanics*, Vol. 1, No. 6, 1956, p. 607–624. doi: 10.1017/S0022112056000408.
- [3] Keefe, "An investigation of the fluctuating forces acting on a stationary circular cylinder in a subsonic stream and of the

**Table 5 Coefficients for the coherence function  $L_g(\text{St})$ , rectangular sections.**

$i$	1	2	3	4	5	6	
$10 \times 10$ (AR = 1)							
20 m/s	$m_i$	$1.21 \times 10^0$	3.787	1.900	1.056	-	-
	$\kappa_i$	$1.26 \times 10^0$	0.949	0.804	0.733	-	-
	$\psi_i$	$8.20 \times 10^0$	190.246	103.504	66.736	-	-
	$\varepsilon_i$	0.239	0.920	0.778	0.538	-	-
	$p_i$	0.000	0.126	0.251	0.377	-	-
40 m/s	$m_i$	$3.86 \times 10^2$	5.334	2.405	1.208	-	-
	$\kappa_i$	$3.81 \times 10^{17}$	0.961	0.865	0.903	-	-
	$\psi_i$	$5.43 \times 10^{17}$	255.806	117.963	113.276	-	-
	$\varepsilon_i$	0.024	0.674	0.747	0.864	-	-
	$p_i$	0.000	0.126	0.251	0.377	-	-
$10 \times 20$ (AR = 2)							
20 m/s	$m_i$	$6.31 \times 10^0$	3.819	41.971	11.031	2.008	1.625
	$\kappa_i$	$2.76 \times 10^0$	0.935	1.229	0.965	1.286	0.594
	$\psi_i$	$3.54 \times 10^1$	90.949	4727.229	144.747	125.171	234.401
	$\varepsilon_i$	0.737	0.887	0.314	0.765	0.347	0.116
	$p_i$	0.000	0.062	0.081	0.141	0.220	0.280
40 m/s	$m_i$	$3.53 \times 10^0$	14.542	6.787	1.570	-	-
	$\kappa_i$	$6.52 \times 10^{-1}$	1.221	1.153	0.962	-	-
	$\psi_i$	$6.40 \times 10^1$	214.602	84.837	29.328	-	-
	$\varepsilon_i$	1.291	0.645	0.826	0.386	-	-
	$p_i$	0.000	0.077	0.146	0.225	-	-
$10 \times 30$ (AR = 3)							
20 m/s	$m_i$	$4.00 \times 10^4$	17.876	5.218	-	-	-
	$\kappa_i$	$1.31 \times 10^8$	1.441	1.589	-	-	-
	$\psi_i$	$2.44 \times 10^8$	252.929	416.854	-	-	-
	$\varepsilon_i$	0.068	0.766	1.398	-	-	-
	$p_i$	0.000	0.163	0.323	-	-	-
40 m/s	$m_i$	$9.51 \times 10^{11}$	24.308	9.953	-	-	-
	$\kappa_i$	$5.32 \times 10^{27}$	1.160	1.476	-	-	-
	$\psi_i$	$2.10 \times 10^{30}$	358.578	454.424	-	-	-
	$\varepsilon_i$	0.025	0.747	1.620	-	-	-
	$p_i$	0.000	0.160	0.319	-	-	-

associated sound field (UTIA REPORT NO. 76),” Tech. rep., Institute of Aerophysics, University of Toronto (UTIA), 1961.

- [4] Becker, S., Hahn, C., Kaltenbacher, M., and Lerch, R., “Flow-Induced Sound of Wall-Mounted Cylinders with Different Geometries,” *AIAA Journal*, Vol. 46, No. 9, 2008, pp. 2265–2281. doi:10.2514/1.34865, URL <https://doi.org/10.2514/>

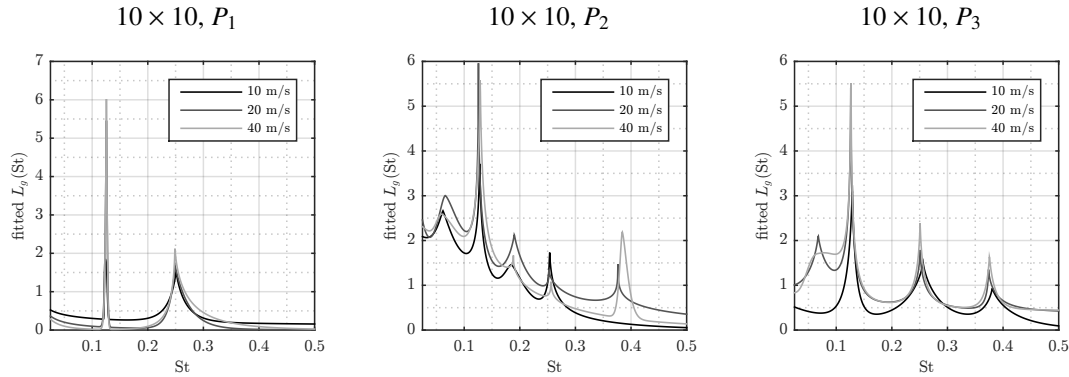


**Fig. 22** Regression laws  $L_g(St)$  for the square section at multiple velocities,  $P_1$  to  $P_3$ .

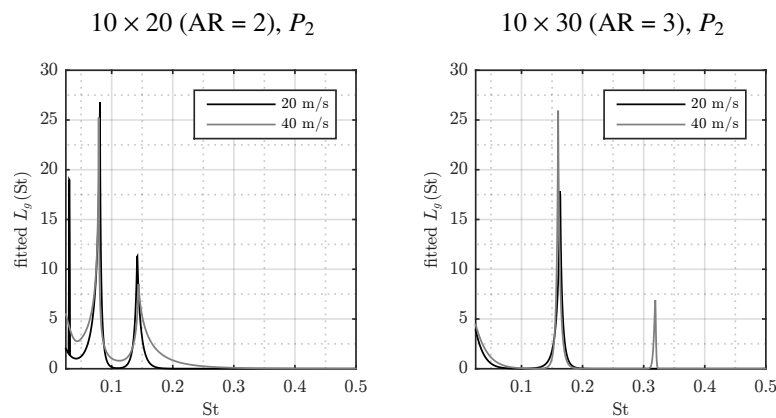


**Fig. 23** Regression laws  $L_g(St)$  for the rectangular sections ( $AR = 2$  and  $AR = 3$ ) at multiple velocities,  $P_2$ .

1.34865.

- [5] King, W., and Pfizenmaier, E., "An experimental study of sound generated by flows around cylinders of different cross-section," *Journal of Sound and Vibration*, Vol. 328, No. 3, 2009, pp. 318 – 337. doi:<https://doi.org/10.1016/j.jsv.2009.07.034>, URL <http://www.sciencedirect.com/science/article/pii/S0022460X09006221>.
- [6] Moreau, D. J., and Doolan, C. J., "Flow-Induced Sound of Wall-Mounted Finite Length Cylinders," *AIAA Journal*, Vol. 51, No. 10, 2013, pp. 2493–2502. doi:10.2514/1.j052391, URL <https://doi.org/10.2514/1.J052391>.
- [7] Iglesias, E. L., Thompson, D., and Smith, M., "Experimental study of the aerodynamic noise radiated by cylinders with different cross-sections and yaw angles," *Journal of Sound and Vibration*, Vol. 361, 2016, pp. 108 – 129. doi:<https://doi.org/10.1016/j.jsv.2015.09.044>, URL <http://www.sciencedirect.com/science/article/pii/S0022460X15007841>.
- [8] Iglesias, E. L., Thompson, D., and Smith, M., "Component-based model to predict aerodynamic noise from high-speed train pantographs," *Journal of Sound and Vibration*, Vol. 394, 2017, pp. 280 – 305. doi:<https://doi.org/10.1016/j.jsv.2017.01.028>, URL <http://www.sciencedirect.com/science/article/pii/S0022460X17300512>.
- [9] Octavianty, R., Asai, M., and Inasawa, A., "Experimental Study on Vortex Shedding and Sound Radiation from a Rectangular Cylinder at Low Mach Numbers," *Transactions of the Japan Society for Aeronautical and Space Sciences*, Vol. 59, No. 5, 2016, pp. 261–268. doi:10.2322/tjsass.59.261.
- [10] Fujita, H., "The characteristics of the Aeolian tone radiated from two-dimensional cylinders," *Fluid Dynamics Research*, Vol. 42, No. 1, 2010, p. 015002. URL <http://stacks.iop.org/1873-7005/42/i=1/a=015002>.
- [11] Lighthill, M. J., "The Bakerian Lecture, 1961 Sound generated aerodynamically," *Proceedings of the Royal Society of London. Series A. Mathematical and Physical Sciences*, Vol. 267, No. 1329, 1962, pp. 147–182. doi:10.1098/rspa.1962.0090, URL <https://royalsocietypublishing.org/doi/abs/10.1098/rspa.1962.0090>.

- [12] Inasawa, A., Asai, M., and Nakano, T., "Sound generation in the flow behind a rectangular cylinder of various aspect ratios at low Mach numbers," *Computers & Fluids*, Vol. 82, No. Supplement C, 2013, pp. 148 – 157. doi:<https://doi.org/10.1016/j.compfluid.2013.05.006>, URL <http://www.sciencedirect.com/science/article/pii/S0045793013001928>.
- [13] Pinto, W. J. G. S., Margnat, F., and Gervais, Y., "Influence of cross-section on the aeolian tone: a numerical study in the laminar regime," *25th AIAA/CEAS Aeroacoustics Conference (Aeroacoustics 2019)*, 20-24 May, Delft, The Netherlands, 2019.
- [14] Okajima, A., "Strouhal numbers of rectangular cylinders," *Journal of Fluid Mechanics*, Vol. 123, 1982, p. 379–398. doi:10.1017/S0022112082003115.
- [15] Knisely, C., "Strouhal numbers of rectangular cylinders at incidence: A review and new data," *Journal of Fluids and Structures*, Vol. 4, No. 4, 1990, pp. 371 – 393. doi:[https://doi.org/10.1016/0889-9746\(90\)90137-T](https://doi.org/10.1016/0889-9746(90)90137-T), URL <http://www.sciencedirect.com/science/article/pii/088997469090137T>.
- [16] Sohankar, A., "Large eddy simulation of flow past rectangular-section cylinders: Side ratio effects," *Journal of Wind Engineering and Industrial Aerodynamics*, Vol. 96, No. 5, 2008, pp. 640 – 655. doi:<https://doi.org/10.1016/j.jweia.2008.02.009>, URL <http://www.sciencedirect.com/science/article/pii/S0167610508000238>.
- [17] Tian, X., Ong, M. C., Yang, J., and Myrhaug, D., "Unsteady RANS simulations of flow around rectangular cylinders with different aspect ratios," *Ocean Engineering*, Vol. 58, 2013, pp. 208 – 216. doi:<https://doi.org/10.1016/j.oceaneng.2012.10.013>, URL <http://www.sciencedirect.com/science/article/pii/S0029801812003976>.
- [18] Ribeiro, J. L. D., "Fluctuating lift and its spanwise correlation on a circular cylinder in a smooth and in a turbulent flow: a critical review," *Journal of Wind Engineering and Industrial Aerodynamics*, Vol. 40, No. 2, 1992, pp. 179 – 198. doi:[https://doi.org/10.1016/0167-6105\(92\)90364-G](https://doi.org/10.1016/0167-6105(92)90364-G), URL <http://www.sciencedirect.com/science/article/pii/016761059290364G>.
- [19] Norberg, C., "Fluctuating lift on a circular cylinder: review and new measurements," *Journal of Fluids and Structures*, Vol. 17, No. 1, 2003, pp. 57 – 96. doi:[https://doi.org/10.1016/S0889-9746\(02\)00099-3](https://doi.org/10.1016/S0889-9746(02)00099-3), URL <http://www.sciencedirect.com/science/article/pii/S0889974602000993>.
- [20] Pinto, W. J. G. S., and Margnat, F., "Experimental study of the influence of cross section shape on spanwise coherence length in flow around cylinders," *under consideration for publication*, 2019.
- [21] Seo, J. H., and Moon, Y. J., "Aerodynamic noise prediction for long-span bodies," *Journal of Sound and Vibration*, Vol. 306, No. 3, 2007, pp. 564 – 579. doi:<https://doi.org/10.1016/j.jsv.2007.05.042>, URL <http://www.sciencedirect.com/science/article/pii/S0022460X07004130>.
- [22] Kato, C., Iida, A., Takano, Y., Fujita, H., and Ikegawa, M., "Numerical prediction of aerodynamic noise radiated from low Mach number turbulent wake," *Aerospace Sciences Meetings, American Institute of Aeronautics and Astronautics*, 1993. doi:10.2514/6.1993-145, URL <https://doi.org/10.2514/6.1993-145>.
- [23] Pérot, F., Gloerfelt, X., Bailly, C., Auger, J.-M., and Giardi, H., "Numerical Prediction of the Noise Radiated by a Cylinder," *Aeroacoustics Conferences, American Institute of Aeronautics and Astronautics*, 2003. doi:10.2514/6.2003-3240, URL <https://doi.org/10.2514/6.2003-3240>.
- [24] Doolan, C. J., "Computational bluff body aerodynamic noise prediction using a statistical approach," *Applied Acoustics*, Vol. 71, No. 12, 2010, pp. 1194 – 1203. doi:<https://doi.org/10.1016/j.apacoust.2010.08.004>, URL <http://www.sciencedirect.com/science/article/pii/S0003682X10001908>.
- [25] Haramoto, Y., Matsuzaki, K., Munekata, M., and Ohba, H., "Emitted Sound From Inclined Circular Cylinder And Three-Dimensional Flow Structure In Wake," *The Twelfth International Offshore and Polar Engineering Conference*, 2002. URL <https://doi.org/>.
- [26] Casalino, D., and Jacob, M., "Prediction of aerodynamic sound from circular rods via spanwise statistical modelling," *Journal of Sound and Vibration*, Vol. 262, No. 4, 2003, pp. 815 – 844. doi:[https://doi.org/10.1016/S0022-460X\(02\)01136-7](https://doi.org/10.1016/S0022-460X(02)01136-7), URL <http://www.sciencedirect.com/science/article/pii/S0022460X02011367>.
- [27] Sueki, T., Takaishi, T., Ikeda, M., and Arai, N., "Application of porous material to reduce aerodynamic sound from bluff bodies," *Fluid Dynamics Research*, Vol. 42, No. 1, 2010, p. 015004. URL <http://stacks.iop.org/1873-7005/42/i=1/a=015004>.
- [28] Norberg, C., "Flow around rectangular cylinders: Pressure forces and wake frequencies," *Journal of Wind Engineering and Industrial Aerodynamics*, Vol. 49, No. 1, 1993, pp. 187 – 196. doi:[https://doi.org/10.1016/0167-6105\(93\)90014-F](https://doi.org/10.1016/0167-6105(93)90014-F), URL <http://www.sciencedirect.com/science/article/pii/016761059390014F>.

- [29] Hutcheson, F. V., and Brooks, T. F., "Noise Radiation from Single and Multiple Rod Configurations," *International Journal of Aeroacoustics*, Vol. 11, No. 3-4, 2012, pp. 291–333. doi:10.1260/1475-472X.11.3-4.291, URL <https://doi.org/10.1260/1475-472X.11.3-4.291>.
- [30] Orselli, R., Meneghini, J., and Saltara, F., "Two and Three-Dimensional Simulation of Sound Generated by Flow Around a Circular Cylinder," *Aeroacoustics Conferences*, American Institute of Aeronautics and Astronautics, 2009. doi:10.2514/6.2009-3270, URL <https://doi.org/10.2514/6.2009-3270>.
- [31] Nelder, J. A., and Mead, R., "A Simplex Method for Function Minimization," *The Computer Journal*, Vol. 7, No. 4, 1965, pp. 308–313. doi:10.1093/comjnl/7.4.308, URL <https://dx.doi.org/10.1093/comjnl/7.4.308>.
- [32] Sohankar, A., "Flow over a bluff body from moderate to high Reynolds numbers using large eddy simulation," *Computers & Fluids*, Vol. 35, No. 10, 2006, pp. 1154 – 1168. doi:<https://doi.org/10.1016/j.compfluid.2005.05.007>, URL <http://www.sciencedirect.com/science/article/pii/S004579300500099X>.
- [33] Bai, H., and Alam, M. M., "Dependence of square cylinder wake on Reynolds number," *Physics of Fluids*, Vol. 30, No. 1, 2018, p. 015102. doi:10.1063/1.4996945, URL <https://doi.org/10.1063/1.4996945>.
- [34] Margnat, F., "Hybrid prediction of the aerodynamic noise radiated by a rectangular cylinder at incidence," *Computers & Fluids*, Vol. 109, 2015, pp. 13 – 26. doi:<http://dx.doi.org/10.1016/j.compfluid.2014.12.006>, URL <http://www.sciencedirect.com/science/article/pii/S0045793014004691>.
- [35] West, G., and Apelt, C., "Fluctuating lift and drag forces on finite lengths of a circular cylinder in the subcritical Reynolds number range," *Journal of Fluids and Structures*, Vol. 11, No. 2, 1997, pp. 135 – 158. doi:<https://doi.org/10.1006/jfls.1996.0070>, URL <http://www.sciencedirect.com/science/article/pii/S0889974696900705>.
- [36] Norberg, C., "Flow around a circular cylinder: aspects of fluctuating lift," *Journal of Fluids and Structures*, Vol. 15, No. 3, 2001, pp. 459 – 469. doi:<https://doi.org/10.1006/jfls.2000.0367>, URL <http://www.sciencedirect.com/science/article/pii/S0889974600903670>.
- [37] Sakamoto, H., Haniu, H., and Kobayashi, Y., "Fluctuating Forces Acting on Rectangular Cylinders in Uniform Flow : On Rectangular Cylinders with Fully Separated Flow (in Japanese)," *Transactions of the Japan Society of Mechanical Engineers Series B*, Vol. 55, No. 516, 1989, pp. 2310–2317. doi:10.1299/kikaib.55.2310.
- [38] Trias, F., Gorobets, A., and Oliva, A., "Turbulent flow around a square cylinder at Reynolds number 22,000: A DNS study," *Computers & Fluids*, Vol. 123, 2015, pp. 87 – 98. doi:<https://doi.org/10.1016/j.compfluid.2015.09.013>, URL <http://www.sciencedirect.com/science/article/pii/S0045793015003254>.
- [39] Tamura, T., and Itoh, Y., "Aerodynamic characteristics and flow structures around a rectangular cylinder with a section of various depth/breadth ratios (in Japanese)," *Journal of Structural and Construction Engineering (Transactions of AIJ)*, Vol. 61, No. 486, 1996, pp. 153–162. doi:10.3130/aijs.61.153\_2.
- [40] Ranjan, P., and Dewan, A., "Effect of side ratio on fluid flow and heat transfer from rectangular cylinders using the PANS method," *International Journal of Heat and Fluid Flow*, Vol. 61, 2016, pp. 309 – 322. doi:<https://doi.org/10.1016/j.ijheatfluidflow.2016.05.004>, URL <http://www.sciencedirect.com/science/article/pii/S0142727X1630162X>.
- [41] Namiranian, F., and Gartshore, I., "Direct measurements of oscillating lift on a rigid square section cylinder in a turbulent stream," *Journal of Wind Engineering and Industrial Aerodynamics*, Vol. 28, No. 1, 1988, pp. 209 – 218. doi:[https://doi.org/10.1016/0167-6105\(88\)90117-1](https://doi.org/10.1016/0167-6105(88)90117-1), URL <http://www.sciencedirect.com/science/article/pii/0167610588901171>.
- [42] McLean, I., and Gartshore, I., "Spanwise correlations of pressure on a rigid square section cylinder," *Journal of Wind Engineering and Industrial Aerodynamics*, Vol. 41, No. 1, 1992, pp. 797 – 808. doi:[https://doi.org/10.1016/0167-6105\(92\)90498-Y](https://doi.org/10.1016/0167-6105(92)90498-Y), URL <http://www.sciencedirect.com/science/article/pii/016761059290498Y>.
- [43] Gioria, R., Meneghini, J., Aranha, J., Barbeiro, I., and Carmo, B., "Effect of the domain spanwise periodic length on the flow around a circular cylinder," *Journal of Fluids and Structures*, Vol. 27, No. 5, 2011, pp. 792 – 797. doi:<https://doi.org/10.1016/j.jfluidstructs.2011.03.007>, URL <http://www.sciencedirect.com/science/article/pii/S0889974611000363>, iUTAM Symposium on Bluff Body Wakes and Vortex-Induced Vibrations (BBVIV-6).
- [44] Mueller, A., "Large Eddy Simulation of cross-flow around a square rod at incidence with application to tonal noise prediction," Ph.D. thesis, University of Twente, Netherlands, 1 2012.

- [45] Kacker, S. C., Pennington, B., and Hill, R. S., "Fluctuating Lift Coefficient for a Circular Cylinder in Cross Flows," *Journal of Mechanical Engineering Science*, Vol. 16, No. 4, 1974, pp. 215–224. doi:10.1243/JMES\_JOUR\_1974\_016\_040\_02, URL [https://doi.org/10.1243/JMES\\_JOUR\\_1974\\_016\\_040\\_02](https://doi.org/10.1243/JMES_JOUR_1974_016_040_02).
- [46] Szepessy, S., and Bearman, P. W., "Aspect ratio and end plate effects on vortex shedding from a circular cylinder," *Journal of Fluid Mechanics*, Vol. 234, 1992, p. 191–217. doi:10.1017/S0022112092000752.
- [47] Blackburn, H. M., and Melbourne, W. H., "The effect of free-stream turbulence on sectional lift forces on a circular cylinder," *Journal of Fluid Mechanics*, Vol. 306, 1996, p. 267–292. doi:10.1017/S0022112096001309.
- [48] Szepessy, "On the control of circular cylinder flow by end plates," *European Journal of Mechanics*, Vol. 12, No. 2, 1993, pp. 217–244.
- [49] Norberg, C., "An experimental investigation of the flow around a circular cylinder: influence of aspect ratio," *Journal of Fluid Mechanics*, Vol. 258, 1994, p. 287–316. doi:10.1017/S0022112094003332.
- [50] Schewe, G., "On the force fluctuations acting on a circular cylinder in crossflow from subcritical up to transcritical Reynolds numbers," *Journal of Fluid Mechanics*, Vol. 133, 1983, p. 265–285. doi:10.1017/S0022112083001913.
- [51] Nishimura, H., and Taniike, Y., "Aerodynamic characteristics of fluctuating forces on a circular cylinder," *Journal of Wind Engineering and Industrial Aerodynamics*, Vol. 89, No. 7, 2001, pp. 713 – 723. doi:[https://doi.org/10.1016/S0167-6105\(01\)00067-8](https://doi.org/10.1016/S0167-6105(01)00067-8), URL <http://www.sciencedirect.com/science/article/pii/S0167610501000678>, 10th International Conference on Wind Engineering.
- [52] Islam, S. U., Zhou, C. Y., Shah, A., and Xie, P., "Numerical simulation of flow past rectangular cylinders with different aspect ratios using the incompressible lattice Boltzmann method," *Journal of Mechanical Science and Technology*, Vol. 26, No. 4, 2012, pp. 1027–1041. doi:10.1007/s12206-012-0328-4, URL <https://doi.org/10.1007/s12206-012-0328-4>.
- [53] Steggel, N., "A Numerical Investigation of the Flow Around Rectangular Cylinders," Ph.D. thesis, University of Surrey, 1998. URL <http://epubs.surrey.ac.uk/id/eprint/771936>.
- [54] Sohankar, A., Norberg, C., and Davidson, L., "A numerical Study of Unsteady Two-Dimensional Flow Around Rectangular Cylinders at Incidence," Tech. Rep. Internal Report Nr. 96/25, Departement of Thermo and Fluid Dynamics, Chalmers University of Technology, 1996.
- [55] Sohankar, A., Norberg, C., and Davidson, L., "Numerical simulation of unsteady low-Reynolds number flow around rectangular cylinders at incidence," *Journal of Wind Engineering and Industrial Aerodynamics*, Vol. 69-71, 1997, pp. 189 – 201. doi:[https://doi.org/10.1016/S0167-6105\(97\)00154-2](https://doi.org/10.1016/S0167-6105(97)00154-2), URL <http://www.sciencedirect.com/science/article/pii/S0167610597001542>, proceedings of the 3rd International Colloquium on Bluff Body Aerodynamics and Applications.
- [56] Tamura, T., and Itoh, Y., "Unstable aerodynamic phenomena of a rectangular cylinder with critical section," *Journal of Wind Engineering and Industrial Aerodynamics*, Vol. 83, No. 1, 1999, pp. 121 – 133. doi:[https://doi.org/10.1016/S0167-6105\(99\)00066-5](https://doi.org/10.1016/S0167-6105(99)00066-5), URL <http://www.sciencedirect.com/science/article/pii/S0167610599000665>.
- [57] Mannini, C., "Applicability of URANS and DES Simulations of Flow Past Rectangular Cylinders and Bridge Sections," *Computation*, Vol. 3, No. 3, 2015, pp. 479–508. doi:10.3390/computation3030479, URL <http://www.mdpi.com/2079-3197/3/3/479>.
- [58] Shimada, K., and Ishihara, T., "Application of a modified k-epsilon model to the prediction of aerodynamic characteristics of rectangular cross-section cylinders," *Journal of Fluids and Structures*, Vol. 16, No. 4, 2002, pp. 465 – 485. doi:<https://doi.org/10.1006/jfls.2001.0433>, URL <http://www.sciencedirect.com/science/article/pii/S0889974601904335>.
- [59] Leehey, P., and Hanson, C., "Aeolian tones associated with resonant vibration," *Journal of Sound and Vibration*, Vol. 13, No. 4, 1970, pp. 465 – 483. doi:[https://doi.org/10.1016/S0022-460X\(70\)80052-9](https://doi.org/10.1016/S0022-460X(70)80052-9), URL <http://www.sciencedirect.com/science/article/pii/S0022460X70800529>.
- [60] Williamson, C. H. K., "Vortex Dynamics in the Cylinder Wake," *Annual Review of Fluid Mechanics*, Vol. 28, No. 1, 1996, pp. 477–539. doi:10.1146/annurev.fl.28.010196.002401, URL <https://doi.org/10.1146/annurev.fl.28.010196.002401>.
- [61] Zdravkovich, M., "Review and classification of various aerodynamic and hydrodynamic means for suppressing vortex shedding," *Journal of Wind Engineering and Industrial Aerodynamics*, Vol. 7, No. 2, 1981, pp. 145 – 189. doi:[https://doi.org/10.1016/0167-6105\(81\)90036-2](https://doi.org/10.1016/0167-6105(81)90036-2), URL <http://www.sciencedirect.com/science/article/pii/0167610581900362>.